From molecular systems to continuum solids: A multiscale structure and dynamics

Qi Tong and Shaofan Li

Citation: The Journal of Chemical Physics **143**, 064101 (2015); doi: 10.1063/1.4927656
View online: http://dx.doi.org/10.1063/1.4927656
View Table of Contents: http://scitation.aip.org/content/aip/journal/jcp/143/6?ver=pdfcov
Published by the AIP Publishing

From molecular systems to continuum solids: A multiscale structure and dynamics

Qi Tong and Shaofan Li[a)]
Department of Civil and Environmental Engineering, University of California, Berkeley, California 94720, USA

(Received 3 May 2015; accepted 20 July 2015; published online 10 August 2015)

We propose a concurrent multiscale molecular dynamics for molecular systems in order to apply macroscale mechanical boundary conditions such as traction and average displacement for solid state materials, which is difficult to do in traditional molecular dynamics where boundary conditions are applied in terms of forces and displacements on selected particles. The multiscale model is systematically constructed in terms of multiscale structures of kinematics, force field, and dynamical equations. The idea is to extend the Anderson-Parrinello-Rahman molecular dynamics to the cases that have arbitrary finite domain and boundary, thus the model is capable of solving inhomogeneous, non-equilibrium problems. The macroscale stress loading on a representative volume element with periodic boundary condition is generalized to all kinds of macroscale mechanical boundary conditions. Unlike most multiscale techniques, our theory is aimed at understanding fundamental physics rather than achieving computing efficiency. Examples of problems with prescribed average displacements and surface tractions are presented to demonstrate the validity of the proposed multiscale molecular dynamics. © *2015 AIP Publishing LLC.* [http://dx.doi.org/10.1063/1.4927656]

I. INTRODUCTION

Many problems in different fields of science and engineering have multiscale characters in space and time.[1–3] They are fascinating, while at the same time post great challenge to modern science and technology. Multiscale simulation, which is often mentioned as a computational terminology, has attracted extensive effort of research during the past decades due to the limitation of single-scale models. Those models are generally categorized either as hierarchical or as concurrent. Hierarchical approach attempts to obtain information from lower scales and directly apply it to higher scales. It is a one direction message-passing procedure without interactive communication or feedback between different scales. Molecular Dynamics (MD)[4] is essentially a hierarchical model, where interatomic potentials can be obtained from underlying quantum mechanical calculation such as the density functional theory.[5,6] Similarly, in various coarse grain models,[7,8] it is often the case that a subscale cluster is subjected to atomistic simulations to determine the nature of the intramolecular potentials. In concurrent methodology, on the other hand, different scales are strongly coupled and solved simultaneously. The interscale dependence is complex, and frequent feedback is desired to pass information between scales. The concurrent multiscale model usually does not require *a priori* knowledge of the macroscale physical variables, which is more suitable for solving complicated cross-scale problems such as inhomogeneous deformation and material defects. Quasi-continuum method[9,10] is an extensively studied and mentioned concurrent model in the literature, which mixes atomistic and continuum models by intentionally eliminating unnecessary degrees of freedom. Coupled atomistic and discrete dislocation methods[11,12] found their success in dislocation simulation by developing schemes for detecting and converting atomistic dislocations to discrete dislocations in continuum field. Other newly developed models include bridging scale method,[13,14] atomistic field theory,[15,16] perfectly matched multiscale method,[17,18] etc.

However, while most multiscale models put efforts on improving efficiency and saving computing resources, physical issues are usually left behind, e.g., ghost force on interface in quasi-continuum model.[19] Artificial assumptions are made to patch the gap between different scales, which gives rise to unphysical consequences. Typically, communication or message passing between scales has two directions: bottom-up and top-down. In the bottom-up approach, atomistic information passes from lower microscopic level to higher macroscopic scale. This approach is relatively straightforward and well studied, where the effort is put on collecting information from lower levels and properly analyzing and interpreting it to describe higher-level phenomena. Statistical mechanics[20] is one of the most important methodologies in this category, whose objective is to extrapolate macroscale quantities such as temperature and pressure based on atomistic positions and velocities in a statistical ensemble. On the other hand, the top-down message-passing approach, i.e., searching optimal state of a molecular system with certain macroscale information, is not thoroughly studied. More specifically, the response of atoms and molecules in microscopic resolution under macroscale boundary condition is not well characterized. The obstacle lies in the fact that macroscopic theories in higher level scale usually introduce empirical assumptions such as continuum deformation and constitutive law rather than deriving them from first principle. Those assumptions simplify the model

a)Electronic address: shaofan@berkeley.edu

and provide intuitive interpretation, which are most useful to solve problems in a single scale but at the cost of losing connection to lower scales. As a matter of fact, any technique that attempts to directly incorporate macroscale theories into atomistic scales would bring in unphysical results due to those artificial assumptions.

This work is aimed at characterizing the motion of molecular systems when macroscale boundary conditions are enforced, i.e., the top-down approach, which is necessary and nontrivial. We focus on macroscale mechanical boundary conditions such as surface tractions and average surface displacements in this paper. Even if we have sufficient computer resources and capacity, which may enable us to calculate macroscale problems with atomistic precision, realistic problems still cannot be properly solved by using the classical molecular dynamics. Because boundary conditions in macroscale are in statistical senses, and they may not be easily incorporated into classical molecular dynamics. For example, in experiments, surface traction is a continuous distribution, and the average boundary displacement is the displacement of the center of a cluster of particles around the boundary of the molecular system domain. But in classical molecular dynamics, we can only apply forces or displacements on selected particles, which is a strong boundary condition compared to macroscale boundary conditions. In an experiment or any engineering activity, controlling a single atom is difficult or even impossible. Thus, numerical simulation of classical molecular dynamics may not be reliable for predicting experimental results. Early attempts to incorporate macroscale quantities into molecular system were made by Anderson in 1980s[21] when he proposed an isoenthalpic-isobaric ensemble molecular dynamics allowing a representative cubic lattice cell to change its volume. Pressure is naturally applied to the lattice cell by introducing external potential energy. Later on, Parrinello and Rahman[22,23] extended Andersen's model to anisotropic cases by varying the shape of the lattice cell in addition to volume. Their model allows macroscale stress loading in molecular dynamical simulation and it is proved to be effective in simulation of phase transition for crystal lattice under constant stress. The Anderson-Parrinello-Rahman Molecular Dynamics (APR-MD) may be viewed as a top-down approach, and its simulation cell is a representative volume element with periodical boundary condition. This model is suitable for simulating homogeneous lattice deformation and internal motion. In APR-MD, the overall motion of the entire cell and the interplay with environment are unspecified due to periodical assumption. Therefore, in a broader scope of realistic macroscale simulation, this model is limited and incapable of inhomogeneous and non-equilibrium problems such as stress distribution or lattice defect motion, e.g., dislocation dynamics.

To reach the goal of complete top-down characterization, a very first step is to construct a multiscale structure where the information is totally based on lower scale without any higher-level assumption. While at the same time, all desired quantities in different scales should be included in the model with clear physical connection. Based on these considerations and inspired by the Anderson-Parrinello-Rahman molecular dynamics, we propose a systematic multiscale mechanical model which consists of three main part:

First, we reveal the fundamental multiscale structure and kinematics for deformable solids from the atomistic framework to macroscale continuum mechanics. We organize the information from the molecular system but observe them from the viewpoint of continuum mechanics. As in continuum mechanics, we center the study on the object of "material point." Its motion includes rigid body translation, rotation, and deformation. However, the proposed multiscale model covers fully the atomistic resolution. For a single "material point," it may be a cluster of atoms and has internal degrees of freedom which is different from continuum mechanics. Globally, the "material points" may not be continuously connected to each other as assumed in continuum mechanics. Consequently, our view of kinematics is no more restricted in each single scale as continuous deformation or atomistic motion.

Second, properly characterize the force fields for the multiscale system. Different force spectrums can be found when we consider both atomistic scale and macroscale space. For example, force field in molecular system is the interactions among atoms and molecules. But in macroscale, force field is continuously represented as surface traction or body force. We intend to put them together in a same multiscale framework.

Third and the most important, describe the motion for the multiscale system by discovering driving force for each scale and deriving dynamic equations. By virtue of the proposed multiscale structure and force field, we are able to put quantities of different scales in a systematic dynamical framework and introduce all kinds of macroscale boundary conditions into molecular systems.

The paper is organized in eight sections. In Section II, we reveal an intrinsic multiscale structure of a class of molecular systems, and discuss the kinematics of each scale. In Section III, we characterize the force field and obtain the associated potential energy. In Section IV, we justify and make comments on the Parrinello-Rahman statistical assumptions. In Section V, the equations of motion will be derived and macroscale boundary conditions will be discussed. Technical aspects are presented in Section VI, including constraints, time integration, and temperature control. We shall validate the multiscale theory by numerical examples of phase transition with both surface traction and displacement boundary conditions. In Section VIII, we close presentation with discussion and comments.

II. MULTISCALE STRUCTURE AND KINEMATICS

The basic thermodynamics ensemble unit in macroscale solid mechanics is a "material point" at which we can define stress and strain, and the material in a continuum body filled the entire domain of space it occupies. However, materials in microscopic scale are basically atoms and molecules separated in space, and these basic units are approximated as particles in molecular dynamics. To find the connection between these two scales, a good starting point is introducing deformable "material point" into microscopic resolution.

As shown in Fig. 1, a molecular system Ω is subjected to macroscale boundary conditions as surface traction $\bar{\mathbf{t}}$ and boundary displacement $\bar{\mathbf{u}}$. We divide the system into several supercells Ω_α. Each supercell is a cluster of atoms or molecules.

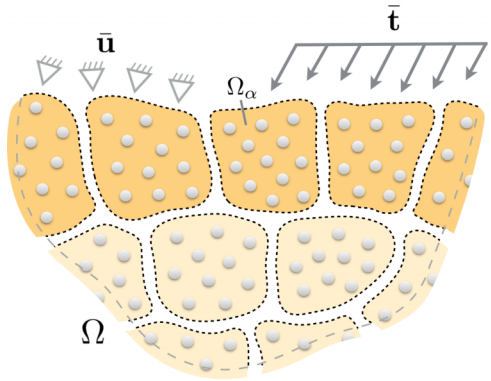

FIG. 1. A molecular system is divided to several supercells. Each supercell is a "material point" standing on the level of macroscale continuum mechanics. The decomposition $\mathbf{r}_i = \mathbf{r}_\alpha + \boldsymbol{\phi}_\alpha \cdot \mathbf{s}_i$ gives the atomic positions inside each cell. Boundary cells exposed to surface traction are marked in deep color, while light color is used for interior cells.

This partition enables us to keep track the motion on the level of a supercell due to the relative motion of internal atoms as "deformation." The shapes of the supercells are arbitrary, so that they can be chosen to fit the geometry of surface domain. The size of cells, on the other hand, will be discussed later in Section VI. In this section, we will discuss kinematics from the perspectives of a single supercell and the global system.

We first focus on the kinematic behavior of a generic αth cell. Throughout the paper, we will use Greek letters α and β to index supercells and lower-case letters i and j to index atoms. The motion of a single supercell can be described by **rigid body translation**, **rotation**, and **stretch** which are at macroscale and mesoscale. For the precise definition of macroscale and mesoscale, we will discuss later in the motion of global system. In addition, there are **internal atomistic degrees of freedom** with microscopic resolution. The connection between these motions is found as

$$\mathbf{r}_i(t) = \mathbf{r}_\alpha(t) + \boldsymbol{\phi}_\alpha(t) \cdot \mathbf{s}_i(t), \tag{1}$$

where $\mathbf{r}_i$ is atomistic positions, $\mathbf{r}_\alpha$ is the center of mass of αth cell which is calculated as

$$\mathbf{r}_\alpha = \sum_i m_i \mathbf{r}_i \Big/ \sum_i m_i, \tag{2}$$

with m_i the mass of ith atom in αth cell. The rigid body translation of a supercell can be casted into the motion of the center of mass $\mathbf{r}_\alpha$. $\boldsymbol{\phi}_\alpha$ is the total deformation gradient of αth cell and is uniform throughout the cell. Deformation gradient is a concept introduced from continuum mechanics. It is a tensorial operator that maps the vectors in different configurations, e.g., $d\mathbf{x} = \boldsymbol{\phi}_\alpha \cdot d\mathbf{X}$, where $d\mathbf{x}$ and $d\mathbf{X}$ are vectors in current and referential configurations, respectively. We use "total deformation gradient" here to distinguish it from continuum deformation gradient, because the supercells are not necessary to be connected continuously, there can be gaps or overlaps among cells in atomistic resolution. Mathematically, we may decompose the total deformation gradient $\boldsymbol{\phi}_\alpha$ by the polar decomposition theorem[24] as

$$\boldsymbol{\phi}_\alpha = \mathbf{R}_\alpha \cdot \mathbf{U}_\alpha = \mathbf{V}_\alpha \cdot \mathbf{R}_\alpha. \tag{3}$$

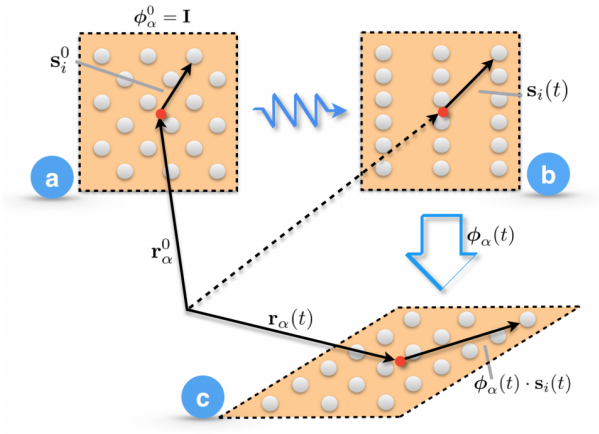

FIG. 2. Evolution of a general cell. Red circle is the center of mass of the cell. (a) is the cell in the referential (initial) configuration; (b) is the intermediate configuration where internal patterns of atomic distribution change but the shape of the cell keeps fixed; (c) is the real physical configuration at current time t. From (b) to (c), the shape change of the cell is described by deformation gradient $\boldsymbol{\phi}_\alpha$. (b) and (c) are at the same time instance but in different space.

In continuum mechanics,[24] $\mathbf{U}_\alpha$ and $\mathbf{V}_\alpha$ are called *right stretch tensor* and *left stretch tensor*, respectively. $\mathbf{R}_\alpha$ is the *rotation tensor*. Thus, deformation gradient $\boldsymbol{\phi}_\alpha$ describes the rotation and stretch of the supercell. $\mathbf{s}_i$ is the independent local coordinate of ith atom inside the supercell as internal degrees of freedom (DOF) which controls the pattern of atomistic distribution but does not influence the shape of the cell. The product $\boldsymbol{\phi}_\alpha \cdot \mathbf{s}_i$ is interpreted as the relative position to the center of mass.

Fig. 2 demonstrates the procedure of evolution for a generic supercell. (a) is the referential configuration of the cell with quantities marked by superscript "0." For convenience, we may define the initial cell at time $t = 0$ as in the referential configuration, namely, $\mathbf{r}_\alpha^0 = \mathbf{r}_\alpha(0)$, $\boldsymbol{\phi}_\alpha^0 = \boldsymbol{\phi}_\alpha(0)$, and $\mathbf{s}_i^0 = \mathbf{s}_i(0)$. And initial deformation gradient $\boldsymbol{\phi}_\alpha(0)$ can be chosen as identity tensor $\mathbf{I}$. Therefore, $\mathbf{s}_i^0$ becomes the relative position in referential configuration as shown in Fig. 2(a). Eq. (1) in referential configuration is then

$$\mathbf{r}_i^0 = \mathbf{r}_\alpha^0 + \boldsymbol{\phi}_\alpha^0 \cdot \mathbf{s}_i^0 = \mathbf{r}_\alpha^0 + \mathbf{s}_i^0. \tag{4}$$

(c) is the current configuration of the cell described by Eq. (1). However, different from continuum mechanics, (c) and (a) are not directly linked by a deformation gradient. If we observe the particles inside the cell in (a) and (c), respectively, we may find the changes of not only the shape of the cell but also the pattern of atomistic distribution. Thus, we introduce an intermediate configuration (b). In this configuration, the shape of the cell holds while $\mathbf{s}_i(t)$ changes with time. The steps (a) and (b) modify the internal distribution, but we cannot see it at the level of macroscale. Step from (b) to (c) is then the standard procedure of macroscale deformation as in continuum mechanics. Note that the deformation is uniform for the whole cell. Also note that (b) configuration is "artificial" which is not really existed, and its time instance is overlapped with (c), which means (b) and (c) are at the same time but in different spaces. In summary, $\mathbf{s}_i(t)$ represents the internal degrees of freedom which controls the atomistic distribution, while $\boldsymbol{\phi}_\alpha(t)$ controls the deformation of the whole supercell.

Next, we discuss the motion of the global system, i.e., the relative displacements and deformations among cells. Since we did not enforce any continuum restriction on supercells, the motion is totally independent on each other. However, if we are interested in extracting or applying continuum deformation to the molecular system, we can further decompose $\boldsymbol{\phi}_\alpha(t)$ as

$$\boldsymbol{\phi}_\alpha(t) = \boldsymbol{\chi}_\alpha(t) \cdot \mathbf{F}_\alpha(t), \tag{5}$$

where $\mathbf{F}_\alpha$ describes the continuum deformation, and $\boldsymbol{\chi}_\alpha$ is the independent cell rotation and distortion. With given boundary geometry, distribution of centers of mass, and continuum restriction, deformation gradient $\mathbf{F}_\alpha$ is uniquely determined. We write it as $\mathbf{F}_\alpha = \mathbf{F}_\alpha(\{\mathbf{r}_\beta\})$, where $\{\mathbf{r}_\beta\}$ means the set of all centers of mass. We use β to distinguish it from the generic cell α under study. We categorize the independent deformation $\boldsymbol{\chi}_\alpha$ as mesoscale motion.

Fig. 3 schematically depicts the deformation of the system on macroscale and mesoscale levels (only rigid body translation, rotation, and stretch are showed in the figure, internal degrees of freedom are smoothed out). The total deformation gradient $\boldsymbol{\phi}_\alpha$ consists of a macro-deformation $\mathbf{F}_\alpha$ and meso-deformation $\boldsymbol{\chi}_\alpha$. Configuration in Fig. 3(a) is the undeformed system. From (a) to (b), with the mapping of $\mathbf{F}_\alpha$, the cells are deformed but still connected to each other without gaps or overlaps due to the continuum restriction on macroscale. From (b) to (c), the mesoscale deformation $\boldsymbol{\chi}_\alpha$ brings in further rotation and stretch to break the connection at macroscale level.

In summary, the proposed model has three scales. Macroscale or continuum scale describes motion of centers of mass $\mathbf{r}_\alpha$ and continuum deformation $\mathbf{F}_\alpha$. They are physically the rigid body translation, continuous rotation, and stretch. The macroscale kinematics may be described by using the language of continuum mechanics. Mesoscale deformation $\boldsymbol{\chi}_\alpha$ further describes the independent distortion of the cells without moving centers of mass. Microscale motion $\mathbf{s}_i$ is the internal DOF which describes the atomistic pattern or distribution. The combination of three scales fully recovers molecular systems without additional assumption. With the decomposition, higher scale quantities are embedded into the molecular system, which gives us insights into the multiscale structure and provides us theoretical guidance to solve cross-scale problems. Usually in continuum mechanics, macroscale boundary conditions are in terms of traction or displacement. We shall discuss how to apply macroscale displacement and traction boundary conditions to molecular dynamics in Section V.

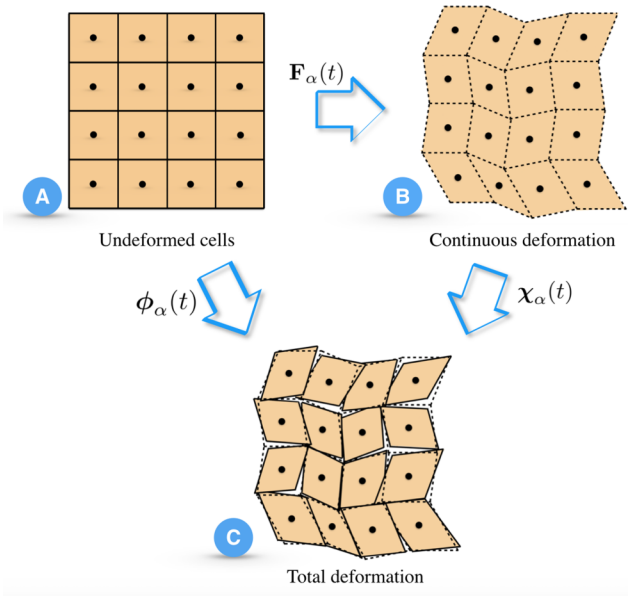

FIG. 3. Macro and meso level deformations: (a) the original undeformed system that is divided into several supercells. The black circles represent the centers of mass; (b) the configuration undergoes macroscale deformation $\mathbf{F}_\alpha$. Note the cells are connected to each other without gaps or overlaps in the framework of continuity, and this deformation is restricted by the relative positions of centers of mass from different cells; (c) the cells further undergo mesoscale deformation $\boldsymbol{\chi}_\alpha$ around their own centers of mass separately without connection. The dashed parallelograms represent the corresponding configuration in (b).

III. POTENTIAL ENERGY AND FORCE FIELD

Fundamentally, forces in a molecular system are interactions among discrete particles. With multiscale structure and kinematics, it is necessary to characterize the force field for supercells in other scales. As has been shown in Fig. 4, for a generic αth cell, the external force field acting on the surface of the cell can be distinguished into two different types. First part is interatomic forces from atoms outside a generic cell which is marked by blue arrows in Fig. 4. This is the fundamental force field on microscale level. Besides interatomic forces, a supercell is sometimes exposed to external loads ideally applied at infinite distance. Loads in this circumstance are in macroscopic scale and usually have the form of surface traction $\bar{\mathbf{t}}_\alpha$ and body force $\bar{\mathbf{b}}_\alpha$.

For the αth cell, separating potential energy to internal part V_α^{int} and external part V_α^{ext}, we define

$$V_\alpha^{int} = \frac{1}{2} \sum_{i,j \in \alpha} \varphi(r_{ij}), \tag{6}$$

where i and j are both indices of atoms inside αth cell, φ is the pair potential, and r_{ij} is the distance between ith and jth atoms. Note that there is a factor of 1/2 because each pair is doubly summated.

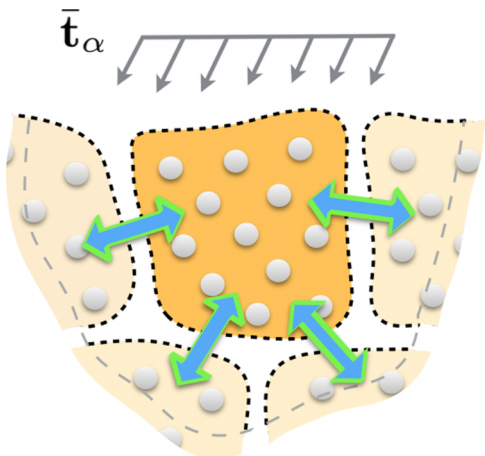

FIG. 4. A supercell is subject to microscale interatomic forces from other cells (blue arrow) and macroscale surface traction $\bar{\mathbf{t}}_\alpha$.

The external potential V_α^{ext} is related to external force field which is contributed by microscale and macroscale sources. The interactions from surrounding particles give

$$V_\alpha^{atom} = \sum_{i\in\alpha, j\notin\alpha} \varphi(r_{ij}). \tag{7}$$

Here, i again is the index of atoms inside the cell, but j is the index of atoms in the neighbor cells. Abbreviation $i \in \alpha$ means that the ith atom belongs to the αth cell, and $j \notin \alpha$ means that the jth atom does not belong to the αth cell. There is no 1/2 factor because each pair is summated once. Both V_α^{int} and V_α^{atom} are in microscale, and they have the same nature of particle interaction. For macroscale surface traction and body force, associated potential energy can be expressed as

$$V_\alpha^{surf} = -S_\alpha^0 \bar{\mathbf{t}}_\alpha^0 \cdot \mathbf{r}_\alpha, \tag{8}$$

$$V_\alpha^{body} = -\Omega_\alpha^0 \bar{\mathbf{b}}_\alpha^0 \cdot \mathbf{r}_\alpha, \tag{9}$$

where S_α^0 is the surface area exposed to $\bar{\mathbf{t}}_\alpha^0$ in the referential configuration. Ω_α^0 is the volume in referential configuration. $\bar{\mathbf{b}}_\alpha^0$ is the applied body force. We use referential quantities to represent dead load. In Eqs. (8) and (9), we apply forces at the center of mass by assuming that higher order terms such as stress couple are negligible. The total external potential for αth supercell reads

$$V_\alpha^{ext} = V_\alpha^{atom} + V_\alpha^{surf} + V_\alpha^{body}. \tag{10}$$

In some cases, we also want to determine stress distribution in simulation domain. If the stress is prescribed, we may introduce the work conjugation of stress and strain. For example, under a prescribed first Piola-Kirchhoff (PK-I) stress $\bar{\mathcal{P}}_\alpha^{ext}$,[24] its work conjugate is the deformation gradient $\boldsymbol{\phi}_\alpha$. We use total deformation instead of continuum deformation because the stress-strain conjugation is based on a single cell. Then, the external potential energy is

$$V_\alpha^{ext} = V_\alpha^{stress} = -\Omega_\alpha^0 \bar{\mathcal{P}}_\alpha^{ext} : \boldsymbol{\phi}_\alpha. \tag{11}$$

Note that V_α^{stress} is a joint effect of all potentials in Eq. (10). However, from solid mechanics, we know that stress state is a macroscale equilibrium concept, i.e., stress can induce deformation but may not cause rigid body translation which requires net force action. Thus, Eq. (11) is valid to derive motion for deformation $\boldsymbol{\phi}_\alpha$ but not for rigid body translation $\mathbf{r}_\alpha$. If we want to use Eq. (11) in the global system, we need to combine it with displacement loading for $\mathbf{r}_\alpha$. More details will be discussed later in Section V. In general, we will use Eq. (10).

Note that all macroscale external forces (traction, body force, and PK-I stress) are in the referential configuration so that they are all dead load. In this way, we can obtain a simple potential energy expression as given in Eqs. (8), (9), and (11). If the external forces are in current configuration and subjected to change with time, the potential energy must be expressed by integration.

IV. KINETIC ENERGY AND STATISTICAL ASSUMPTIONS

With the decomposition in Eq. (1), we have the kinetic energy of the αth cell,

$$\begin{aligned} K_\alpha &= \frac{1}{2}\sum_i m_i \dot{\mathbf{r}}_i \cdot \dot{\mathbf{r}}_i \\ &= \frac{1}{2}\sum_i m_i (\dot{\mathbf{r}}_\alpha + \dot{\boldsymbol{\phi}}_\alpha \cdot \mathbf{s}_i + \boldsymbol{\phi}_\alpha \cdot \dot{\mathbf{s}}_i) \cdot (\dot{\mathbf{r}}_\alpha + \dot{\boldsymbol{\phi}}_\alpha \cdot \mathbf{s}_i + \boldsymbol{\phi}_\alpha \cdot \dot{\mathbf{s}}_i) \\ &= \frac{1}{2} M_\alpha \dot{\mathbf{r}}_\alpha \cdot \dot{\mathbf{r}}_\alpha + \frac{1}{2}\dot{\boldsymbol{\phi}}_\alpha^T \dot{\boldsymbol{\phi}}_\alpha : \sum_i m_i \mathbf{s}_i \otimes \mathbf{s}_i + \frac{1}{2}\mathbf{C}_\alpha : \sum_i m_i \dot{\mathbf{s}}_i \otimes \dot{\mathbf{s}}_i + \frac{1}{2}\dot{\boldsymbol{\phi}}_\alpha^T \boldsymbol{\phi}_\alpha : \sum_i m_i \mathbf{s}_i \otimes \dot{\mathbf{s}}_i + \frac{1}{2}\boldsymbol{\phi}_\alpha^T \dot{\boldsymbol{\phi}}_\alpha : \sum_i m_i \dot{\mathbf{s}}_i \otimes \mathbf{s}_i, \end{aligned} \tag{12}$$

where M_α is the mass of the whole cell; $\mathbf{C}_\alpha = \boldsymbol{\phi}_\alpha^T \boldsymbol{\phi}_\alpha$ is the right Cauchy-Green tensor as introduced in continuum mechanics. Consider representing contributions to kinetic energy by four parts: (1) rigid body translation K_α^{rigid}, (2) cell stretch and rotation K_α^{cell}, (3) internal motion of atoms K_α^{atom}, and (4) mix motion K_α^{mix}. They are read from Eq. (12) and rewritten as

$$\begin{aligned} K_\alpha^{rigid} &= \frac{1}{2} M_\alpha \dot{\mathbf{r}}_\alpha \cdot \dot{\mathbf{r}}_\alpha, \\ K_\alpha^{cell} &= \frac{1}{2}\dot{\boldsymbol{\phi}}_\alpha^T \dot{\boldsymbol{\phi}}_\alpha : \sum_i m_i \mathbf{s}_i \otimes \mathbf{s}_i = \frac{1}{2}\dot{\boldsymbol{\phi}}_\alpha^T \dot{\boldsymbol{\phi}}_\alpha : \mathbf{J}_\alpha, \\ K_\alpha^{atom} &= \frac{1}{2}\mathbf{C}_\alpha : \sum_i m_i \dot{\mathbf{s}}_i \otimes \dot{\mathbf{s}}_i, \\ K_\alpha^{mix} &= \frac{1}{2}\dot{\boldsymbol{\phi}}_\alpha^T \boldsymbol{\phi}_\alpha : \sum_i m_i \mathbf{s}_i \otimes \dot{\mathbf{s}}_i + \frac{1}{2}\boldsymbol{\phi}_\alpha^T \dot{\boldsymbol{\phi}}_\alpha : \sum_i m_i \dot{\mathbf{s}}_i \otimes \mathbf{s}_i, \end{aligned} \tag{13}$$

where $\mathbf{J}_\alpha = \sum_i m_i \mathbf{s}_i \otimes \mathbf{s}_i$ is defined as inertia tensor.

Next, we discuss two statistical assumptions which are originally implied by Parrinello and Rahman[22,23] but unexplained. We render brief physical interpretations and basic mathematical justifications.

Assumption I. Inertial tensor $\mathbf{J}_\alpha$ can be approximated as a constant.

This assumption implies that the density distribution does not change significantly. For instance, if particles initially concentrated around the center of mass tend to move outward, the value of $\mathbf{J}_\alpha$ will increase. We demonstrate this point by choosing principal axes $\mathbf{e}_1$, $\mathbf{e}_2$, and $\mathbf{e}_3$, and express $\mathbf{J}_\alpha$ as

$$\mathbf{J}_\alpha = J_{11}\mathbf{e}_1 \otimes \mathbf{e}_1 + J_{22}\mathbf{e}_2 \otimes \mathbf{e}_2 + J_{33}\mathbf{e}_3 \otimes \mathbf{e}_3, \tag{14}$$

with $J_{11} = \sum_i m_i s_{i1}^2$, $J_{22} = \sum_i m_i s_{i2}^2$, and $J_{33} = \sum_i m_i s_{i3}^2$. We can see that these values are basically density distribution along each direction. The farther particles located away from the

center of mass, the bigger $\mathbf{J}_\alpha$ is. For a homogeneous cell, Assumption I always holds.

It should be noted that in PR-MD, $\mathbf{J}_\alpha$ is a spherical tensor, namely, $J_{11} = J_{22} = J_{33} = W$ and thus, $\mathbf{J}_\alpha = W\mathbf{I}$, with W a constant. This is because $\mathbf{s}_i$ space is homogeneous and **cubic**, namely, the range of $\mathbf{s}_i$ on each direction is the same and normalized as [0, 1]. However, this is not the case in our cells. $\mathbf{s}_i$ in our model is a vector in real physical space which is not normalized. Therefore, arbitrary selection of shape may result in polarization of $\mathbf{J}_\alpha$.

From the above discussion, one can see that Assumption I can simplify the model, and it is best suited for a homogeneous cell. We must carefully use it in applications for inhomogeneous cases.

Assumption II. The mixed kinetic energy K_{mix} is negligible compared to other kinetic energies.

Consider the following correlation function:

$$\mathbf{AC}(\tau) = \langle \mathbf{s}_i(t) \otimes \mathbf{s}_i(t+\tau) \rangle = \sum_i m_i \mathbf{s}_i(t) \otimes \mathbf{s}_i(t+\tau), \tag{15}$$

where τ is an infinite small time increment. Atomistic motion includes two parts: vibration around instant equilibrium positions with finite temperature and lattice displacement (polarization) under external force field. As shown in Fig. 5, blue arrows represent lattice displacements, and atomistic vibration are modeled by springs connected between atoms. Atomistic vibration is much faster than lattice displacement. Therefore, in the neighborhood of time instant t, lattice displacement is negligible and only atomistic vibration is in scope. Statistically, for a cluster of particles vibrating around the equilibrium positions, we state without proof that the correlation function is approximately a constant of τ in the neighborhood of t; thus,

$$\sum_i m_i \mathbf{s}_i(t) \otimes \mathbf{s}_i(t+\tau) \approx \sum_i m_i \mathbf{s}_i(t) \otimes \mathbf{s}_i(t). \tag{16}$$

Thus, the time derivation of correlation function is zero at $\tau = 0$, which is

$$\frac{d}{d\tau}\mathbf{AC}|_{\tau=0} = \sum_i m_i \mathbf{s}_i(t) \otimes \dot{\mathbf{s}}_i(t) = 0. \tag{17}$$

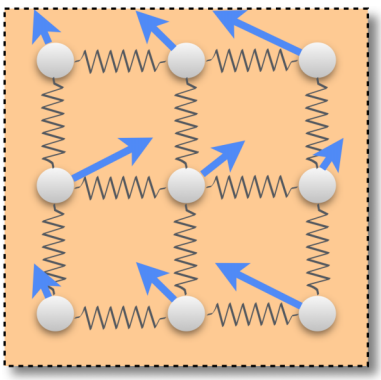

FIG. 5. Atomic vibration and polarization. Atoms are vibrating rapidly around their instant equilibrium lattice positions. This motion is modeled by springs and rigid balls. Under external force field, equilibrium positions change slowly in the long term.

Similarly,

$$\sum_i m_i \dot{\mathbf{s}}_i(t) \otimes \mathbf{s}_i(t) = 0. \tag{18}$$

Comparing with Eq. (13), we have $K_\alpha^{mix} = 0$. Consequently, kinetic energy is decoupled and only separate terms K_α^{rigid}, K_α^{cell}, and K_α^{atom} are left. This simplification makes the kinetic energy clearly associate with motions in different scales.

We rewrite kinetic energy as

$$\begin{aligned} K_\alpha &= K_\alpha^{rigid} + K_\alpha^{cell} + K_\alpha^{atom} \\ &= \frac{1}{2} M_\alpha \dot{\mathbf{r}}_\alpha \cdot \dot{\mathbf{r}}_\alpha + \frac{1}{2} \dot{\boldsymbol{\phi}}_\alpha^T \dot{\boldsymbol{\phi}}_\alpha : \mathbf{J}_\alpha + \frac{1}{2} \mathbf{C}_\alpha : \sum_i m_i \dot{\mathbf{s}}_i \otimes \dot{\mathbf{s}}_i. \end{aligned} \tag{19}$$

V. DYNAMIC EQUATIONS AND MACROSCALE BOUNDARY CONDITIONS

In this section, we shall obtain equations of motion for independent variables $\mathbf{r}_\alpha$, $\boldsymbol{\phi}_\alpha$, and $\mathbf{s}_i$ based on Lagrangian $\mathcal{L}_\alpha = \mathcal{L}_\alpha(\mathbf{r}_\alpha, \boldsymbol{\phi}_\alpha, \mathbf{s}_i)$. If we introduce continuum deformation $\mathbf{F}_\alpha$, $\boldsymbol{\chi}_\alpha$ as a component of $\boldsymbol{\phi}_\alpha$ can be chosen as an independent variable because $\mathbf{F}_\alpha$ is totally determined by centers of mass $\mathbf{r}_\alpha$. We will show that the multiplicative decomposition $\boldsymbol{\phi}_\alpha = \boldsymbol{\chi}_\alpha \cdot \mathbf{F}_\alpha$ does not influence the equation of motion for $\mathbf{r}_\alpha$ even with the dependency of $\mathbf{F}_\alpha$. Based on the derivations in Secs. III and IV, we write the Lagrangian for αth cell as

$$\begin{aligned} \mathcal{L}_\alpha &= K_\alpha - V_\alpha \\ &= K_\alpha^{rigid} + K_\alpha^{cell} + K_\alpha^{atom} - V_\alpha^{int} - V_\alpha^{ext} \\ &= \frac{1}{2} M_\alpha \dot{\mathbf{r}}_\alpha \cdot \dot{\mathbf{r}}_\alpha + \frac{1}{2} \dot{\boldsymbol{\phi}}_\alpha^T \dot{\boldsymbol{\phi}}_\alpha : \mathbf{J}_\alpha + \frac{1}{2} \mathbf{C}_\alpha : \sum_i m_i \dot{\mathbf{s}}_i \otimes \dot{\mathbf{s}}_i \\ &\quad - \frac{1}{2} \sum_{i,j \in \alpha} \varphi(r_{ij}) - \sum_{i \in \alpha, j \notin \alpha} \varphi(r_{ij}) \\ &\quad + S_\alpha^0 \bar{\mathbf{t}}_\alpha^0 \cdot \mathbf{r}_\alpha + \Omega_\alpha^0 \bar{\mathbf{b}}_\alpha^0 \cdot \mathbf{r}_\alpha. \end{aligned} \tag{20}$$

The last two terms as external potential energy bring macroscale information into the molecular system. The standard procedure to derive equations of motion is stated as follows,

$$\frac{d}{dt}\frac{\partial \mathcal{L}_\alpha}{\partial \dot{\mathbf{r}}_\alpha} - \frac{\partial \mathcal{L}_\alpha}{\partial \mathbf{r}_\alpha} = 0, \tag{21}$$

$$\frac{d}{dt}\frac{\partial \mathcal{L}_\alpha}{\partial \dot{\boldsymbol{\phi}}_\alpha} - \frac{\partial \mathcal{L}_\alpha}{\partial \boldsymbol{\phi}_\alpha} = 0, \tag{22}$$

$$\frac{d}{dt}\frac{\partial \mathcal{L}_\alpha}{\partial \dot{\mathbf{s}}_i} - \frac{\partial \mathcal{L}_\alpha}{\partial \mathbf{s}_i} = 0. \tag{23}$$

First, we consider the motion of cell centers $\mathbf{r}_\alpha$. We have

$$\frac{d}{dt}\left(\frac{\partial \mathcal{L}_\alpha}{\partial \dot{\mathbf{r}}_\alpha}\right) = M_\alpha \ddot{\mathbf{r}}_\alpha \tag{24}$$

and

$$\begin{aligned} \frac{\partial \mathcal{L}_\alpha}{\partial \mathbf{r}_\alpha} &= -\frac{1}{2} \sum_{i,j \in \alpha} \varphi'(r_{ij}) \frac{\mathbf{r}_{ij}}{r_{ij}} \cdot \frac{\partial \mathbf{r}_{ij}}{\partial \mathbf{r}_\alpha} \\ &\quad - \sum_{i \in \alpha, j \notin \alpha} \varphi'(r_{ij}) \frac{\mathbf{r}_{ij}}{r_{ij}} \cdot \frac{\partial \mathbf{r}_{ij}}{\partial \mathbf{r}_\alpha} + S_\alpha^0 \bar{\mathbf{t}}_\alpha^0 + \Omega_\alpha^0 \bar{\mathbf{b}}_\alpha^0 \\ &= \sum_{i \in \alpha, j \notin \alpha} \mathbf{f}_{ij} + S_\alpha^0 \bar{\mathbf{t}}_\alpha^0 + \Omega_\alpha^0 \bar{\mathbf{b}}_\alpha^0 \end{aligned} \tag{25}$$

by utilizing the relation

$$\frac{\partial \mathbf{r}_{ij}}{\partial \mathbf{r}_\alpha} = \begin{cases} -\mathbf{I} & i \in \alpha, j \notin \alpha \\ \mathbf{0} & i,j \in \alpha \end{cases}, \tag{26}$$

where $\mathbf{I}$ is the second order identity tensor. $\varphi'(r_{ij})\hat{\mathbf{r}}_{ij} = \mathbf{f}_{ij}$, where $\hat{\mathbf{r}}_{ij} = \mathbf{r}_{ij}/r_{ij}$ is the unit vector point from ith atom to jth atom; $\mathbf{r}_{ij} = \mathbf{r}_j - \mathbf{r}_i$; $r_{ij} = |\mathbf{r}_{ij}|$; $\mathbf{f}_{ij}$ is the pair force acting on ith atom by jth atom. Note that the sign of $\mathbf{f}_{ij}$ is the same as $\hat{\mathbf{r}}_{ij}$ when r_{ij} is larger than the equilibrium distance and opposite to $\hat{\mathbf{r}}_{ij}$ when r_{ij} is smaller than the equilibrium distance. Thus, the dynamic equation for $\mathbf{r}_\alpha$ is

$$M_\alpha \ddot{\mathbf{r}}_\alpha = \sum_{i\in\alpha, j\notin\alpha} \mathbf{f}_{ij} + S^0_\alpha \bar{\mathbf{t}}^0_\alpha + \Omega^0_\alpha \bar{\mathbf{b}}^0_\alpha. \tag{27}$$

The driving force for cell centers $\mathbf{r}_\alpha$ consists of three parts: interaction from external particles, surface traction, and body force.

We also want to know the effect when introducing the decomposition $\boldsymbol{\phi}_\alpha = \boldsymbol{\chi}_\alpha \cdot \mathbf{F}_\alpha$, with $\mathbf{F}_\alpha$ depending on $\mathbf{r}_\alpha$. In this case, the terms in dynamic equations are

$$\frac{d}{dt}\left(\frac{\partial \mathcal{L}_\alpha}{\partial \dot{\mathbf{r}}_\alpha}\right) = \frac{d}{dt}\left(\frac{\partial \mathcal{L}_\alpha}{\partial \dot{\mathbf{r}}_\alpha} + \frac{\partial \mathcal{L}_\alpha}{\partial \dot{\boldsymbol{\phi}}_\alpha} \cdot \frac{\partial \dot{\boldsymbol{\phi}}_\alpha}{\partial \dot{\mathbf{r}}_\alpha}\right), \tag{28}$$

$$\frac{\partial \mathcal{L}_\alpha}{\partial \mathbf{r}_\alpha} = \frac{\partial \mathcal{L}_\alpha}{\partial \mathbf{r}_\alpha} + \frac{\partial \mathcal{L}_\alpha}{\partial \boldsymbol{\phi}_\alpha} \cdot \frac{\partial \boldsymbol{\phi}_\alpha}{\partial \mathbf{r}_\alpha} + \frac{\partial \mathcal{L}_\alpha}{\partial \dot{\boldsymbol{\phi}}_\alpha} \cdot \frac{\partial \dot{\boldsymbol{\phi}}_\alpha}{\partial \mathbf{r}_\alpha}. \tag{29}$$

We will reach exactly the same equation as (27), which means that introducing continuum deformation does not influence rigid body translation. And continuum deformation is merely a part of the independent motion of the whole system. Details of derivation is presented in the Appendix.

Then, we derive the dynamic equation for $\boldsymbol{\phi}_\alpha$. We have

$$\frac{d}{dt}\left(\frac{\partial \mathcal{L}_\alpha}{\partial \dot{\boldsymbol{\phi}}_\alpha}\right) = \frac{d}{dt}\left(\dot{\boldsymbol{\phi}}_\alpha \cdot \mathbf{J}_\alpha\right) = \ddot{\boldsymbol{\phi}}_\alpha \cdot \mathbf{J}_\alpha \tag{30}$$

and

$$\begin{aligned}\frac{\partial \mathcal{L}_\alpha}{\partial \boldsymbol{\phi}_\alpha} &= \boldsymbol{\phi}_\alpha \cdot \sum_i m_i \dot{\mathbf{s}}_i \otimes \dot{\mathbf{s}}_i - \frac{1}{2}\sum_{i,j\in\alpha} \varphi'(r_{ij})\frac{\mathbf{r}_{ij}}{r_{ij}} \cdot \frac{\partial \mathbf{r}_{ij}}{\partial \boldsymbol{\phi}_\alpha} \\ &\quad - \sum_{i\in\alpha, j\notin\alpha} \varphi'(r_{ij})\frac{\mathbf{r}_{ij}}{r_{ij}} \cdot \frac{\partial \mathbf{r}_{ij}}{\partial \boldsymbol{\phi}_\alpha} \\ &= \boldsymbol{\phi}_\alpha \cdot \sum_i m_i \dot{\mathbf{s}}_i \otimes \dot{\mathbf{s}}_i - \frac{1}{2}\sum_{i,j\in\alpha} \mathbf{f}_{ij} \otimes \mathbf{s}_{ij} + \sum_{i\in\alpha, j\notin\alpha} \mathbf{f}_{ij} \otimes \mathbf{s}_i,\end{aligned} \tag{31}$$

where $\mathbf{s}_{ij} = \mathbf{s}_j - \mathbf{s}_i$. Note the net forces $S^0_\alpha \bar{\mathbf{t}}^0_\alpha$ and $\Omega^0_\alpha \bar{\mathbf{b}}^0_\alpha$ do not influence the motion of $\boldsymbol{\phi}_\alpha$.

We define the internal and external first PK-I stresses as

$$\mathcal{P}^{int}_\alpha = \frac{1}{\Omega^0_\alpha}\left(\frac{1}{2}\sum_{i,j\in\alpha} \mathbf{f}_{ij} \otimes \mathbf{s}_{ij} - \phi_\alpha \cdot \sum_{i\in\alpha} m_i \dot{\mathbf{s}}_i \otimes \dot{\mathbf{s}}_i\right), \tag{32}$$

$$\mathcal{P}^{ext}_\alpha = \frac{1}{\Omega^0_\alpha}\sum_{i\in\alpha, j\notin\alpha} \mathbf{f}_{ij} \otimes \mathbf{s}_i. \tag{33}$$

The dynamic equation for $\boldsymbol{\phi}_\alpha$ can be written as

$$\ddot{\boldsymbol{\phi}}_\alpha \cdot \mathbf{J}_\alpha = \left(\mathcal{P}^{ext}_\alpha - \mathcal{P}^{int}_\alpha\right)\Omega^0_\alpha. \tag{34}$$

$\mathcal{P}^{int}_\alpha$ is the resistance stress compared with the driving stress $\mathcal{P}^{ext}_\alpha$, so that it comes with a minus sign. When they reach a balance, $\boldsymbol{\phi}_\alpha$ is in equilibrium value.

We know in continuum mechanics that PK-I stress is defined from the Cauchy stress $\boldsymbol{\sigma}_\alpha$ as

$$\mathcal{P}_\alpha = det(\boldsymbol{\phi}_\alpha)\boldsymbol{\sigma}_\alpha \cdot \boldsymbol{\phi}^{-T}_\alpha. \tag{35}$$

Comparing with Eqs. (32) and (33), we find that

$$\begin{aligned}\boldsymbol{\sigma}^{int}_\alpha &= \frac{1}{det(\boldsymbol{\phi}_\alpha)\Omega^0_\alpha}\left(\frac{1}{2}\sum_{i,j\in\alpha} \mathbf{f}_{ij} \otimes \mathbf{s}_{ij} - \phi_\alpha \cdot \sum_{i\in\alpha} m_i \dot{\mathbf{s}}_i \otimes \dot{\mathbf{s}}_i\right) \cdot \boldsymbol{\phi}^T_\alpha \\ &= \frac{1}{\Omega_\alpha}\left(\frac{1}{2}\sum_{i,j\in\alpha} \mathbf{f}_{ij} \otimes \mathbf{r}_{ij} - \sum_{i\in\alpha} m_i(\phi_\alpha \cdot \dot{\mathbf{s}}_i) \otimes (\phi_\alpha \cdot \dot{\mathbf{s}}_i)\right),\end{aligned} \tag{36}$$

$$\begin{aligned}\boldsymbol{\sigma}^{ext}_\alpha &= \frac{1}{det(\boldsymbol{\phi}_\alpha)\Omega^0_\alpha}\sum_{i\in\alpha, j\notin\alpha} \mathbf{f}_{ij} \otimes \mathbf{s}_i \cdot \boldsymbol{\phi}^T_\alpha \\ &= \frac{1}{\Omega_\alpha}\sum_{i\in\alpha, j\notin\alpha} \mathbf{f}_{ij} \otimes \mathbf{r}_i,\end{aligned} \tag{37}$$

which are internal and external Cauchy stresses.

Since $\mathbf{r}_\alpha$, $\boldsymbol{\phi}_\alpha$, and $\mathbf{s}_i$ are in different time scales, i.e., $\Delta t_{\mathbf{r}_\alpha} > \Delta t_{\phi_\alpha} \gg \Delta t_{\mathbf{s}_i}$, therefore, we can define the fine scale velocity as $\dot{\mathbf{r}}_{i'} = \boldsymbol{\phi}_\alpha \cdot \dot{\mathbf{s}}_i$. Eq. (36) can be written as

$$\boldsymbol{\sigma}^{int}_\alpha = \frac{1}{\Omega_\alpha}\left(\frac{1}{2}\sum_{i,j\in\alpha} \mathbf{f}_{ij} \otimes \mathbf{r}_{ij} - \sum_{i\in\alpha} m_i \dot{\mathbf{r}}'_i \otimes \dot{\mathbf{r}}'_i\right) \tag{38}$$

which is the definition of the Virial stress,[25] i.e., $\boldsymbol{\sigma}^{int}_\alpha = \boldsymbol{\sigma}^{Virial}_\alpha$. Apparently, microscale atomistic velocity plays a role in the macroscale stress. Connecting a supercell to a material point in continuum mechanics, we conclude that external stress from the environment provides driving force for stretch and rotation of the cell (material point), while the Virial stress serving as the internal stress resists the deformation. They will be balanced when the system is in macroscale and mesoscale equilibria. We can also interpret the external stress as a pure mechanical stress and the internal stress as a combination of mechanical and thermodynamical stresses due to different physical origins.

Next, we derive the equation of motion for $\mathbf{s}_i$,

$$\frac{d}{dt}\left(\frac{\partial \mathcal{L}_\alpha}{\partial \dot{\mathbf{s}}_i}\right) = \frac{d}{dt}\left(m_i \mathbf{C}_\alpha \cdot \dot{\mathbf{s}}_i\right) = m_i \dot{\mathbf{C}}_\alpha \cdot \dot{\mathbf{s}}_i + m_i \mathbf{C}_\alpha \cdot \ddot{\mathbf{s}}_i \tag{39}$$

and

$$\begin{aligned}\frac{\partial \mathcal{L}_\alpha}{\partial \mathbf{s}_i} &= -\sum_{j\in\alpha} \varphi'(r_{ij})\frac{\mathbf{r}_{ij}}{r_{ij}} \cdot \frac{\partial \mathbf{r}_{ij}}{\partial \mathbf{s}_i} - \sum_{j\notin\alpha} \varphi'(r_{ij})\frac{\mathbf{r}_{ij}}{r_{ij}} \cdot \frac{\partial \mathbf{r}_{ij}}{\partial \mathbf{s}_i} \\ &= \sum_j \mathbf{f}_{ij} \cdot \boldsymbol{\phi}_\alpha.\end{aligned} \tag{40}$$

Note that in the above derivation, the 1/2 factor is gone because the ith atom is summated twice in the internal potential energy term. And since internal and external parts have the same form, we simply combine them. And the dynamic equation is

$$m_i \mathbf{C}_\alpha \cdot \ddot{\mathbf{s}}_i = \sum_j \mathbf{f}_{ij} \cdot \boldsymbol{\phi}_\alpha - m_i \dot{\mathbf{C}}_\alpha \cdot \dot{\mathbf{s}}_i. \tag{41}$$

The first term on the right hand side is the driving force. The second term on the right hand side is associated with both macroscale velocity $\dot{\mathbf{C}}_\alpha$ and microscale velocity $\dot{\mathbf{s}}_i$. Physically,

this is a damping force which resists the motion of $\mathbf{s}_i$, and the motion of the cell serves as a damping coefficient. If the system is in macro and mesoscale equilibrium states, namely, $\dot{\mathbf{C}}_\alpha = 0$, this term is vanished.

So far, we have obtained dynamical equations at different scales: (27), (34), and (41). In summary, we rewrite them together as follows,

$$M_\alpha \ddot{\mathbf{r}}_\alpha = \sum_{i\in\alpha, j\notin\alpha} \mathbf{f}_{ij} + S^0_\alpha \bar{\mathbf{t}}^0_\alpha + \Omega^0_\alpha \bar{\mathbf{b}}^0_\alpha, \tag{42}$$

$$\ddot{\boldsymbol{\phi}}_\alpha \cdot \mathbf{J}_\alpha = \left(\mathcal{P}^{ext}_\alpha - \mathcal{P}^{int}_\alpha\right)\Omega^0_\alpha, \tag{43}$$

$$m_i \mathbf{C}_\alpha \cdot \ddot{\mathbf{s}}_i = \sum_j \mathbf{f}_{ij} \cdot \boldsymbol{\phi}_\alpha - m_i \dot{\mathbf{C}}_\alpha \cdot \dot{\mathbf{s}}_i. \tag{44}$$

They represent coarse scale motion, cell deformation and rotation, internal motion, respectively. The multiscale structure interperates the chaotic motion of molecular system in an organized atomistic-to-continuum viewpoint. As equations of motion, they have the same generalized form $\tilde{M}\ddot{\mathbf{q}} = \tilde{\mathbf{F}}$ with generalized mass M_α, $\mathbf{J}_\alpha$, and $m_i\mathbf{C}_\alpha$. The driving force for rigid body translation is the net force acting on the cell. The motion of deformation and rotation is induced by external stress from the environment and resisted by internal Virial stress. And the internal motion is driven by interactions among particles, while damped due to the existence of cell motions.

To implement dynamical equations for a realistic multiscale system, we need proper boundary conditions. Applying macroscale boundary conditions in molecular systems is a main purpose of the multiscale model. There are four different macroscale boundary conditions:

(I) traction (force) boundary,
(II) displacement boundary,
(III) stress boundary,
(IV) strain boundary.

Boundary conditions (I) and (II) are relatively easier to enforce. For example, we may directly apply surface traction $\bar{\mathbf{t}}^0_\alpha$ or body force $\bar{\mathbf{b}}^0_\alpha$ in Equation (42). The boundary conditions (III) and (IV), on the other hand, usually requires more care. We discuss stress and strain separately.

With the stress boundary condition, boundary cells are controlled by desired stress states. Note that stress state is an equilibrium concept associated with cell deformation, while surface traction or body force is net force to induce rigid body motion. In this case, we take advantage of external potential energy proposed in Eq. (11) and replace the V^{ext}_α in Eq. (20) by V^{stress}_α. After the same procedure of derivation, the dynamic Eq. (34) for $\boldsymbol{\phi}_\alpha$ becomes

$$\ddot{\boldsymbol{\phi}}_\alpha \cdot \mathbf{J}_\alpha = \left(\bar{\mathcal{P}}^{ext}_\alpha - \mathcal{P}^{int}_\alpha\right)\Omega^0_\alpha \tag{45}$$

which has the same form as Eq. (34), but the external PK-I stress is replaced by the prescribed value $\bar{\mathcal{P}}^{ext}_\alpha$. Note that stress boundary alone is not enough to uniquely determine the evolution of the system, because we also need to specify the driving force for rigid body motion.

To apply strain boundary, we may use the continuum deformation $\mathbf{F}_\alpha$ instead of $\boldsymbol{\phi}_\alpha$. For example, $\bar{\mathbf{E}}_\alpha = \frac{1}{2}\left(\bar{\mathbf{F}}^T_\alpha \bar{\mathbf{F}}_\alpha - 1\right)$, where $\bar{\mathbf{E}}_\alpha$ is an applied Green-Lagrangian strain. Thus, applying $\bar{\mathbf{F}}_\alpha$ gives the desired strain. We have mentioned in Section II that $\mathbf{F}_\alpha$ totally depends on the relative positions of centers of mass and boundary geometry, i.e., $\bar{\mathbf{F}}_\alpha = \bar{\mathbf{F}}_\alpha(\{\bar{\mathbf{r}}_\beta\})$. Therefore, strain boundary is in fact equivalent to prescribe the relative positions for the centers of boundary cells and their adjacent cells. However, the relation between $\mathbf{F}_\alpha$ and centers of mass of cells is not a one-to-one map, because there can be rigid body motions of the whole system (different from rigid body motion of a single cell). We still need additional Dirichlet boundary conditions. Approaches to map between $\mathbf{F}_\alpha$ and $\{\mathbf{r}_\beta\}$ will be presented in a separate study for necessary circumstances.

In summary, the Neumann boundary conditions usually need to work together with other boundary conditions, otherwise the evolution of the system may not be unique. In general, we are more interested in the Dirichlet boundary condition (traction and displacement) in realistic dynamical systems.

VI. TECHNICAL ASPECTS

A. Constraints and size dependency

An issue that we have not discussed so far is the constraints of the variables. Recall that in Secs. II–V we have discussed the physical meaning of multiscale kinematic variables: the center of mass $\mathbf{r}_\alpha$, the total deformation gradient $\boldsymbol{\phi}_\alpha$, and internal motion $\mathbf{s}_i$. We may specify them initially, but the physical interpretations are not guaranteed during simulations. Actually, the multiscale decomposition in Eq. (1) is non-unique. For example, at some certain time t, atomic position can be

$$\mathbf{r}_i(t) = \mathbf{r}_\alpha(t) + \boldsymbol{\phi}_\alpha(t)\cdot\mathbf{s}_i(t) = \mathbf{r}^*_\alpha(t) + \boldsymbol{\phi}^*_\alpha(t)\cdot\mathbf{s}^*_i(t) \tag{46}$$

for different sets of $\mathbf{r}_\alpha$, $\boldsymbol{\phi}_\alpha$, and $\mathbf{s}_i$. The real position $\mathbf{r}_i(t)$ is honestly calculated because we did not bring any additional assumption into the model, so that any combination should be equivalent to the original molecular system, i.e., another set $\mathbf{r}^*_\alpha$, $\boldsymbol{\phi}^*_\alpha$, and $\mathbf{s}^*_i$ may give the same $\mathbf{r}_i(t)$. To avoid non-uniqueness, we shall enforce constraints on those variables.

The first constraint is that the physical position of the center of mass must be conserved. With the definition of $\mathbf{r}_\alpha$, we have

$$\begin{aligned}\mathbf{r}_\alpha &= \frac{\sum_i m_i\mathbf{r}_i}{\sum_i m_i} = \frac{1}{M_\alpha}\left(\sum_i m_i\mathbf{r}_\alpha + \sum_i m_i\boldsymbol{\phi}_\alpha\cdot\mathbf{s}_i\right)\\ &= \mathbf{r}_\alpha + \frac{\boldsymbol{\phi}_\alpha}{M_\alpha}\cdot\sum_i m_i\mathbf{s}_i.\end{aligned} \tag{47}$$

The condition to ensure Eq. (47) is

$$\mathbf{G}_1 = \sum_i m_i\mathbf{s}_i(t) = 0. \tag{48}$$

Second, the shape change of the cell must be conserved, i.e., $\boldsymbol{\phi}_\alpha$ always represents the real deformation gradient. The terminology "shape change" means the deformation of a cell without considering internal motion as if the lattice pattern is smoothed out. We may check the configurations in Fig. 6 where (a)-(b)-(c) is the correct mapping process. From (a) to (b), internal pattern of atomic distribution $\mathbf{s}_i$ changes but the overall shape is still the same. With $\boldsymbol{\phi}_\alpha$, (b) is mapped to (c), which is merely the shape change. In another possible undesired path (a)-(d)-(c), where shape of $\mathbf{s}^*_i$ space is different

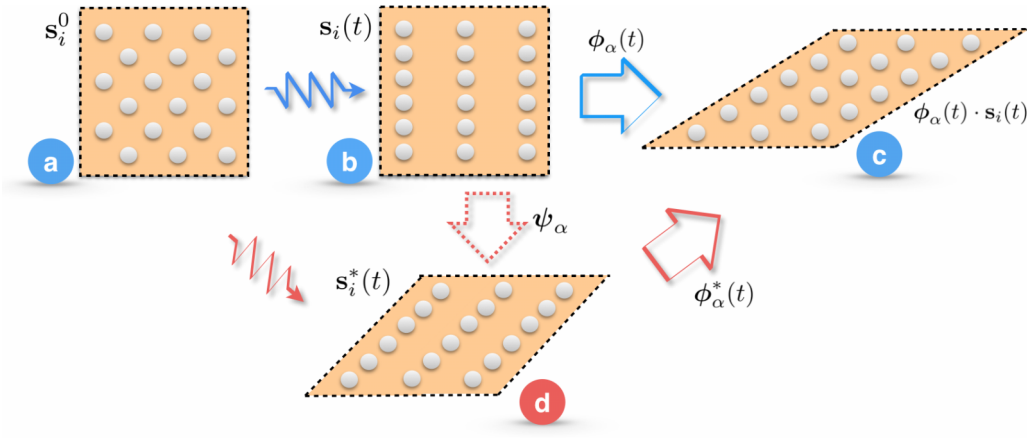

FIG. 6. Possible misinterpretation.

from that of initial $\mathbf{s}_i^0$ space, the operator $\boldsymbol{\phi}_\alpha^*$ is not the true deformation gradient for the cell anymore, which results in misinterpretation.

To resolve this issue, we compare the configurations (b) and (d) in Fig. 6 and introduce an operator $\boldsymbol{\psi}_\alpha$ which gives the mapping,

$$\mathbf{s}_i^* = \boldsymbol{\psi}_\alpha \cdot \mathbf{s}_i, \tag{49}$$

then we have two equivalent paths from (b) to (c), i.e., $\boldsymbol{\phi}_\alpha = \boldsymbol{\phi}_\alpha^* \cdot \boldsymbol{\psi}_\alpha$, and the mapping process of deformation can be further decomposed to

$$\boldsymbol{\phi}_\alpha \cdot \mathbf{s}_i = \boldsymbol{\phi}_\alpha^* \cdot \boldsymbol{\psi}_\alpha \cdot \boldsymbol{\psi}_\alpha^{-1} \cdot \mathbf{s}_i^*. \tag{50}$$

Thus, as long as we can find the operator $\boldsymbol{\psi}_\alpha$, we may pull $\boldsymbol{\phi}_\alpha^*$ back to the desired $\boldsymbol{\phi}_\alpha$. As an example, we may keep track of three critical boundary particles $\mathbf{s}_1$, $\mathbf{s}_2$, and $\mathbf{s}_3$ (e.g., particles around vertices) which are not in a same plane. We assume that the cell shape changes at any time during the simulation as we shall discuss later in this subsection, and $\mathbf{s}_1(t) \approx \mathbf{s}_1^0$, $\mathbf{s}_2(t) \approx \mathbf{s}_2^0$, $\mathbf{s}_3(t) \approx \mathbf{s}_3^0$ for those critical particles. Therefore,

$$[\mathbf{s}_1^* \, \mathbf{s}_2^* \, \mathbf{s}_3^*] = \boldsymbol{\psi}_\alpha \cdot [\mathbf{s}_1 \, \mathbf{s}_2 \, \mathbf{s}_3] \approx \boldsymbol{\psi}_\alpha \cdot [\mathbf{s}_1^0 \, \mathbf{s}_2^0 \, \mathbf{s}_3^0]. \tag{51}$$

Since $\mathbf{s}_1^0$, $\mathbf{s}_2^0$, and $\mathbf{s}_3^0$ are not in a same plane, we can reverse them to obtain $\boldsymbol{\psi}_\alpha$,

$$\boldsymbol{\psi}_\alpha \approx [\mathbf{s}_1^* \, \mathbf{s}_2^* \, \mathbf{s}_3^*] \cdot [\mathbf{s}_1^0 \, \mathbf{s}_2^0 \, \mathbf{s}_3^0]^{-1}. \tag{52}$$

Therefore, if $\boldsymbol{\psi}_\alpha$ is set as identity tensor, i.e., $[\mathbf{s}_1^* \, \mathbf{s}_2^* \, \mathbf{s}_3^*] = [\mathbf{s}_1^0 \, \mathbf{s}_2^0 \, \mathbf{s}_3^0]$, we have $\boldsymbol{\phi}_\alpha = \boldsymbol{\phi}_\alpha^* \cdot \boldsymbol{\psi}_\alpha = \boldsymbol{\phi}_\alpha^*$. To obtain more reliable result, we may choose a group of atoms around $\mathbf{s}_1$, $\mathbf{s}_2$, and $\mathbf{s}_3$ and calculate the average value. This criterion is satisfied for arbitrary shapes of cells. The constraint can be expressed as

$$\mathbf{G}_2 = [\bar{\mathbf{s}}_1^*(t) \, \bar{\mathbf{s}}_2^*(t) \, \bar{\mathbf{s}}_3^*(t)] - [\bar{\mathbf{s}}_1^0 \, \bar{\mathbf{s}}_2^0 \, \bar{\mathbf{s}}_3^0] = 0. \tag{53}$$

Each quantity in the above equation is the average value of a cluster of atoms.

To enforce $\mathbf{G}_1$, we may employ traditional approaches such as Lagrangian multiplier method.[26] The extended Lagrangian for Eq. (20) is

$$\mathcal{L}_\alpha^* = \mathcal{L}_\alpha - \boldsymbol{\lambda} \cdot \mathbf{G}_1, \tag{54}$$

where Lagrangian multiplier $\boldsymbol{\lambda}$ is a vector. The constrained equation of motion for $\mathbf{s}_i$ is

$$\frac{d}{dt}\frac{\partial \mathcal{L}_\alpha^*}{\partial \dot{\mathbf{s}}_i} - \frac{\partial \mathcal{L}_\alpha^*}{\partial \mathbf{s}_i} = 0. \tag{55}$$

Since we know that $\partial \mathbf{G}_1 / \partial \mathbf{s}_i = m_i \mathbf{I}$, then from Equation (55), we have

$$m_i \mathbf{C}_\alpha \cdot \ddot{\mathbf{s}}_i = \sum_j \mathbf{f}_{ij} \cdot \boldsymbol{\phi}_\alpha - m_i \dot{\mathbf{C}}_\alpha \cdot \dot{\mathbf{s}}_i - m_i \boldsymbol{\lambda}. \tag{56}$$

By performing iterative schemes such as SHAKE algorithm,[27] $\mathbf{G}_1$ can be restricted in a given tolerance. The procedure to enforce $\mathbf{G}_2$ is similar.

However, if we exam the problem from a different perspective, we may have better choice to enforce the constraints. Note that the above constraints are in terms of $\mathbf{s}_i$, but the combination of $\mathbf{r}_\alpha$, $\boldsymbol{\phi}_\alpha$, and $\mathbf{s}_i$ is $\mathbf{r}_i$ which is not restricted. Therefore, we can convert the constraint conditions to $\mathbf{r}_\alpha$ and $\boldsymbol{\phi}_\alpha$. The procedure is briefly stated as follows. Step 1: for conservation of the centers of mass, we first assemble real atomistic position $\mathbf{r}_i$ by Equation (46), then calculate the correct center of mass by $\mathbf{r}_\alpha = \sum_i m_i \mathbf{r}_i / \sum_i m_i$. Step 2: for conservation of deformation gradient, we calculate the operator $\boldsymbol{\psi}_\alpha$ by Eq. (52), then perform the operation in (50) to obtain the desired deformation gradient $\boldsymbol{\phi}_\alpha$. We may perform steps 1 and 2 once in every several time steps. This approach is more straightforward and efficient than Lagrangian multiplier method.

Another issue is the supercell size dependency. Intuitively, the size of cells cannot be too big or too small. If it is too small, assumptions in Section IV may not be guaranteed because certain amount of particles are required to ensure that it is statistically meaningful. So that there is a lower bound for cell sizes. On the other hand, we use a unique deformation gradient to track the shapes of supercells. Therefore, cells cannot be too big to include non-unique distortion. That is the upper bound for cell sizes. Typically, the bound may range from a nanometer to hundred nanometers or even bigger, which depends on the problem of interest. We need to perform tests to study the influence of size when dealing with specific problems. For inhomogeneous materials or problems including defects, the size should be relatively small. However, there is no strict requirement on the cell size upper bound. In fact, even if the cell deformation may not be unique due to the large sizes,

the real atomistic position $\mathbf{r}_i$ is not influenced by it as we shall discuss later. Misinterpretation of deformation gradient $\boldsymbol{\phi}_\alpha$ will, at most, make the stress and strain unreliable and the picture of $\boldsymbol{\phi}_\alpha$ ambiguous. For the boundary condition traction or displacement, there is no such confusion because we can always keep track of the centers of mass for different cells, no matter how the shape distorts. In this case, we can neglect the physical picture of $\boldsymbol{\phi}_\alpha$. The theory is still valid. Therefore, the multiscale structure can actually be made adaptive to inhomogeneity and defects with big cells.

B. Time integration

As observed in dynamics equations (42)–(44), quantities $\mathbf{r}_\alpha$, $\boldsymbol{\phi}_\alpha$, and $\mathbf{s}_i$ of multiple spacial and time scales in a same framework are strongly coupled and require intensive message exchange among them. A proper multiscale integration scheme is necessary to aid the communication. Step size of integration for each quantity should be chosen to reflect the time scale variation, i.e., $\Delta t_{\mathbf{r}_\alpha} > \Delta t_{\phi_\alpha} \gg \Delta t_{\mathbf{s}_i}$. The procedure of information exchange among scales is similar to the scheme developed for fluid-structure interaction simulations in Ref. 28, where time step used in fluid is a small fraction of that in solid. We employ the following coupling algorithm in the multiscale integration with serial and parallel approaches, respectively.

The serial computation algorithm is shown in Fig. 7. $\mathbf{r}_\alpha$, $\boldsymbol{\phi}_\alpha$, and $\mathbf{s}_i$ evolve with different time scales and step sizes. (1)–(4) and (5)–(8) are two subcycles in each updating loop. For subcycle (1)–(4), calculation of $\boldsymbol{\phi}_\alpha$ is advanced by Δt_{ϕ_α} for several substeps and pass information back to macroscale for a single step $\mathbf{r}_\alpha$ calculation. Same loop is implemented for subcycle (5)–(8), where $\mathbf{s}_i$ is advanced for several substeps and pass information back for each $\boldsymbol{\phi}_\alpha$ step forward. In serial scheme, when one scale is evolving, quantities in other scales are standing still as "frozen." For parallel computation algorithm, $\mathbf{r}_\alpha$, $\boldsymbol{\phi}_\alpha$, and $\mathbf{s}_i$ advance simultaneously as shown in Fig. 8. The subcycles are observed in (1)–(3) and (4)–(6). On the common starting point of a substep in each scale, information is exchanged among the quantities at the same time instance without lead or lag. Usually, serial algorithm is preferred because parallel algorithm requires smaller step sizes in order to be numerically stable and sufficiently accurate.[28] But parallel algorithm can be naturally incorporated with

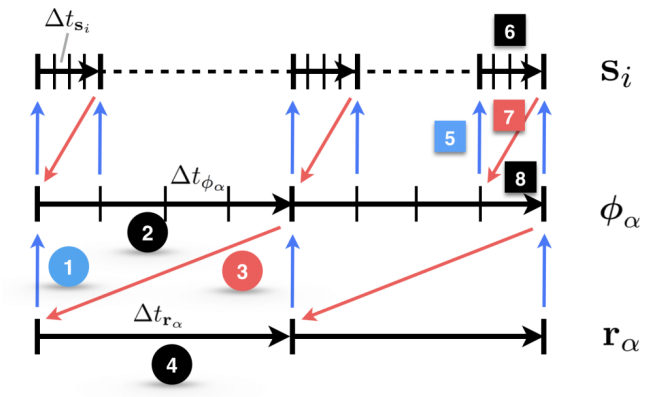

FIG. 7. Serial algorithm for time evolution.

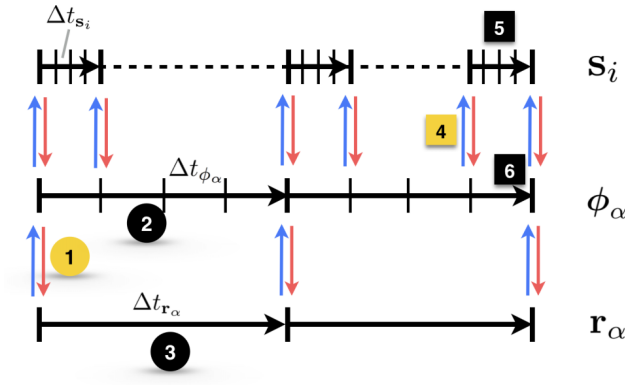

FIG. 8. Parallel algorithm.

parallel computing for multiple CPU cores without additional treatment, which is an advantage in certain cases.

Popular algorithms used in molecular dynamics are the velocity Verlet and the predictor-corrector algorithms. Velocity Verlet[29] is symplectic, time reversible, and it is straightforward to implement, which makes it one of the most widely used algorithms in molecular dynamics. We employ velocity Verlet in calculating macroscale motion $\mathbf{r}_\alpha$. The order of updating time steps is as follows:

$$\mathbf{r}_\alpha^{n+1} = \mathbf{r}_\alpha^n + \dot{\mathbf{r}}_\alpha^n \Delta t_{\mathbf{r}_\alpha} + \frac{1}{2}\ddot{\mathbf{r}}_\alpha^n \Delta t_{\mathbf{r}_\alpha}^2 \tag{57}$$

$$\rightarrow \textit{Evaluate}\ \ \ddot{\mathbf{r}}_\alpha^{n+1},$$

$$\dot{\mathbf{r}}_\alpha^{n+1} = \dot{\mathbf{r}}_\alpha^n + \frac{1}{2}\left(\ddot{\mathbf{r}}_\alpha^n \Delta t_{\mathbf{r}_\alpha} + \ddot{\mathbf{r}}_\alpha^{n+1} \Delta t_{\mathbf{r}_\alpha}\right). \tag{58}$$

The intermediate step of evaluating acceleration is where we need to obtain information from $\boldsymbol{\phi}_\alpha$ and $\mathbf{s}_i$ to assemble $\mathbf{r}_i$ according to Eq. (42). We may choose serial or parallel algorithm for information exchange.

For evolution of $\boldsymbol{\phi}_\alpha$ and $\mathbf{s}_i$, as observed in Equations (43) and (44), the accelerations depend on velocities which are not determined in the step of evaluation if we use velocity Verlet. Instead, we choose standard six order predictor-corrector scheme.[30]

C. Temperature control

In this work, we mainly study the mechanical boundary conditions. All simulations are under controlled temperature, i.e., no heat flow is involved. We leave the heat conduction as a future work. In classical molecular dynamics, a variety of thermostat are introduced in classical molecular dynamics, including Anderson thermostat, Berendsen thermostat, Nosé-Hoover thermostat, and Langevin thermostat. Here, we employ the popular Nosé-Hoover thermostat in our model to control the microscale motion. We develop basic formulation in this subsection.

As stated by Nosé,[31] a new variable w is introduced to exchange heat with the system by scaling velocities. w is interpreted as a time scaling variable as $\Delta t = \Delta t'/w$, where Δt is real time step and $\Delta t'$ is virtual time step. Since the coarse scale velocity varies much slower than that of microscale, as we discussed in Sec. V, the relative velocity can be approximated

as $\dot{\mathbf{r}}_i = \boldsymbol{\phi}_\alpha \cdot \dot{\mathbf{s}}_i$. Therefore, heat transfer primarily influences the velocity of microscale $\dot{\mathbf{s}}_i$. The extended Lagrangian is

$$\mathcal{L}'_\alpha = \frac{1}{2} M_\alpha \dot{\mathbf{r}}_\alpha \cdot \dot{\mathbf{r}}_\alpha + \frac{1}{2} \dot{\boldsymbol{\phi}}_\alpha^T \dot{\boldsymbol{\phi}}_\alpha : \mathbf{J}_\alpha + \frac{1}{2} \mathbf{C}_\alpha : \sum_i m_i w^2 \frac{d\mathbf{s}'_i}{dt'} \otimes \frac{d\mathbf{s}'_i}{dt'} - V_\alpha + \frac{Q}{2} \left(\frac{dw}{dt'} \right)^2 - g k_B T \ln w, \tag{59}$$

where Q is the effective mass of w, g is the number of total degrees of freedom, k_B is Boltzmann constant, and T is the desired temperature. Last two terms are kinetic energy and potential energy for w. Primes denote the quantities and derivatives in virtual time axis. Dots and double dots represent the time derivatives in real axis. Equations of motion for $\mathbf{r}_\alpha$ and $\boldsymbol{\phi}_\alpha$ are the same as in (42) and (43). Dynamic equations of $\mathbf{s}'_i$ and w are derived in virtual time coordinates,

$$\mathbf{C}_\alpha \cdot \frac{d^2 \mathbf{s}'_i}{dt'^2} = \frac{1}{m_i w^2} \sum_j \mathbf{f}_{ij} \cdot \boldsymbol{\phi}_\alpha - \frac{d\mathbf{C}_\alpha}{dt'} \cdot \frac{d\mathbf{s}'_i}{dt'} - 2 \frac{1}{w} \frac{dw}{dt'} \mathbf{C}_\alpha \cdot \frac{d\mathbf{s}'_i}{dt'}, \tag{60}$$

$$Q \frac{d^2 w}{dt'^2} = \mathbf{C}_\alpha : \sum_i m_i w \frac{d\mathbf{s}'_i}{dt'} \otimes \frac{d\mathbf{s}'_i}{dt'} - \frac{g k_B T}{w}. \tag{61}$$

With relations $\Delta t = \Delta t'/w$ and $\mathbf{s}_i = \mathbf{s}'_i$, we may convert the dynamic equations back to real time axis,

$$\mathbf{C}_\alpha \cdot \ddot{\mathbf{s}}_i = \frac{1}{m_i} \sum_j \mathbf{f}_{ij} \cdot \boldsymbol{\phi}_\alpha - \dot{\mathbf{C}}_\alpha \cdot \dot{\mathbf{s}}_i - 2 \frac{\dot{w}}{w} \mathbf{C}_\alpha \cdot \dot{\mathbf{s}}_i, \tag{62}$$

$$Q \ddot{w} = \mathbf{C}_\alpha : \sum_i m_i w \dot{\mathbf{s}}_i \otimes \dot{\mathbf{s}}_i - g k_B T w. \tag{63}$$

With Hoover's modification[32] by introducing a new variable ζ as

$$\zeta = \frac{dw}{dt'} = \frac{\dot{w}}{w}, \quad \dot{\zeta} = \frac{\ddot{w}}{w}. \tag{64}$$

The real-time equations of motion become

$$\mathbf{C}_\alpha \cdot \ddot{\mathbf{s}}_i = \frac{1}{m_i} \sum_j \mathbf{f}_{ij} \cdot \boldsymbol{\phi}_\alpha - \dot{\mathbf{C}}_\alpha \cdot \dot{\mathbf{s}}_i - 2\zeta \mathbf{C}_\alpha \cdot \dot{\mathbf{s}}_i, \tag{65}$$

$$Q \dot{\zeta} = \mathbf{C}_\alpha : \sum_i m_i \dot{\mathbf{s}}_i \otimes \dot{\mathbf{s}}_i - g k_B T. \tag{66}$$

Equations (65) and (66) are used in scaling the microscale quantity for temperature control.

VII. NUMERICAL EXAMPLES

In this section, we present two examples of phase transition with displacement and traction boundary conditions, respectively. Dimensions of the models used in these examples are small, typically within the range of several nanometers, or tens of unit cells of crystal lattice. The purpose of these examples is to verify and demonstrate the multiscale model by applying macroscale boundary conditions in molecular systems, rather than solving realistic large scale problems.

A. Test of displacement boundary condition

The first example is devised to investigate the procedure of phase transit under displacement loading, e.g., uniaxial stretch boundary condition. The model is a finite size bulk nickel with $9 \times 9 \times 9$ unit cells of Face Centered Cubic (F.C.C.) lattice which is shown in Fig. 9(a). The bulk has in total 729 F.C.C. unit cells and 2916 atoms according to basic crystallography. The lattice constant is $a_0 = 0.352$ nm at room temperature, with which the nickel crystal is in a stress free state for infinite lattice. Atomic weight for nickel is 58.69 u. The bulk metal is divided to $3 \times 3 \times 3$ supercells, and each supercell has $3 \times 3 \times 3$ unit cells. The separation ensures that at least one internal supercell is not exposed to boundaries. We may use this cell for benchmark test comparing with known results in infinite lattice. The interaction between atoms is modeled by the Morse potential.[33] It has the form of

$$\varphi(r) = D(e^{-2\alpha(r-r_0)} - 2e^{-\alpha(r-r_0)}). \tag{67}$$

The pair force is given by

$$f(r) = -\frac{\partial \phi(r)}{\partial r} = 2D\alpha(-e^{-2\alpha(r-r_0)} + e^{-\alpha(r-r_0)}), \tag{68}$$

with the constants $D = 3.5059 \times 10^{-20}$ J, $\alpha = 8.766/a_0$, and $r_0 = 0.717\,27$ Å.

During the entire simulation, the temperature is controlled around 350 °K by using the Nosé-Hoover thermostat on microscale motion as formulated in Sec. VI. Before loading, random perturbation of velocities was assigned to get the desired temperature initially. A 5000 free-steps run without any boundary constraint is conducted to get the optimal initial configuration. Subsequently, we apply uniaxial compressive stretches incrementally on y direction which is [010] in F.C.C. lattice as shown in Fig. 9(a). The stretch is realized by moving the centers of mass of top and bottom cells close and then allow them to relax in a time period. The compress-relax procedure gives a certain strain rate. Integration time steps used in simulation are 0.0015 ps, 0.0012 ps, and 0.000 15 ps for different scales. We relax the system for 2000 macro steps for each incremental stretch of 0.03.

Figs. 9(b)–9(d) show the snapshots of structural evolution under different stretches with lateral and top views. When the stretch is relatively small, e.g., $\lambda = 0.92$, the Ni bulk goes through simply elastic deformation. The pattern of particle distribution is still uniform. From both top view and lateral view in Fig. 9(b), we do not observe relative displacements between any adjacent planes. When the stretch increases, e.g., $\lambda = 0.88$, some sort of interplanar slip is activated between the planes of {001} accompanied by the elastic in-plane deformation. As we observe from the top view in Fig. 9(c), the shape is changed from square to parallelogram due to the slip between {001} planes. But the structure at this point is a little bit irregular and unstable. Further increasing the stretch, e.g., $\lambda = 0.77$, the lateral planes {001} get more regular patterns as in closely packed planes {0001} of H.C.P. structure. The final configuration in Fig. 9(e) with $\lambda = 0.72$ is the new stable H.C.P. structure. The lattice constant turns into $a_1 = 0.252$ nm which is approximately $\sqrt{2}/2$ times a_0 and is the same as atomic bond in original F.C.C. configuration.

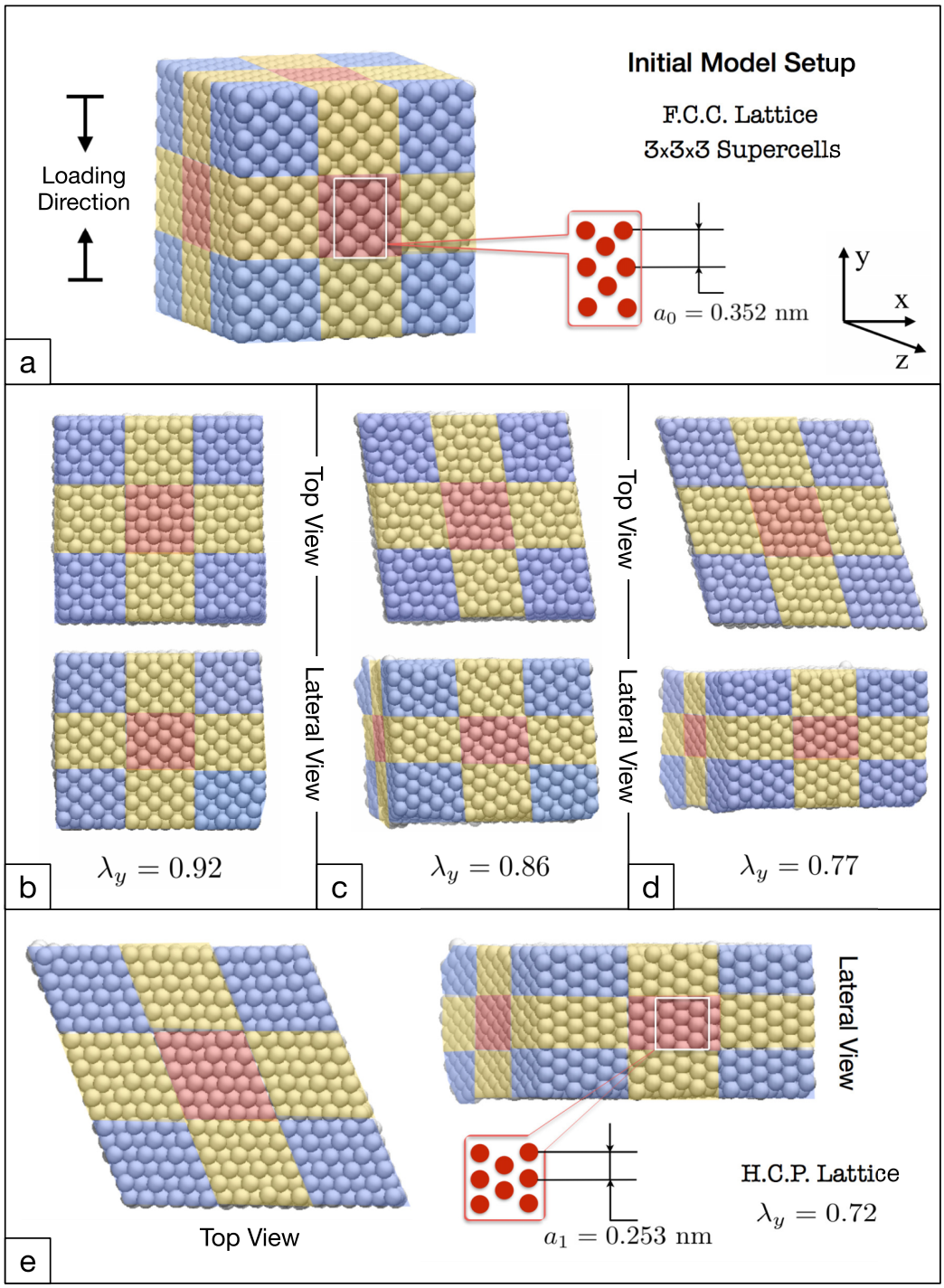

FIG. 9. The model setup and the procedure of structure change under uniaxial displacement loading in [010] direction. The system consists of $3\times3\times3$ supercells, and each supercell consists of $3\times3\times3$ unit cells. We use different colors to distinguish supercells.

We notice that the final H.C.P. configuration of the whole model is regular without boundary distortion, which is different from the results of traditional molecular dynamics. If the displacements are applied on boundary atoms as in molecular dynamics, the structural pattern near the boundary area will be irregular because those atoms are not free to search the optimal positions. By prescribing the displacement for the centers of mass of the boundary supercells relaxes the constraints for specific atoms. Average displacements are enforced as a form of overall rigid body translations for the prescribed cells, while the internal motions are still allowed. This example shows the advantage of the top-down multiscale model in the case of applying macroscale boundary conditions.

We studied the stress-strain relation in a benchmark test to compare it with the theoretical prediction of infinite lattice as reported in Ref. 34. For the model that consists of $3 \times 3 \times 3$ supercells, one may expect that the internal cell is more suitable to approximate the environment of the infinite lattice than boundary cells. We plotted the loading curve from the initial configuration to a stretch around $\lambda = 0.7$. As shown in Fig. 10,

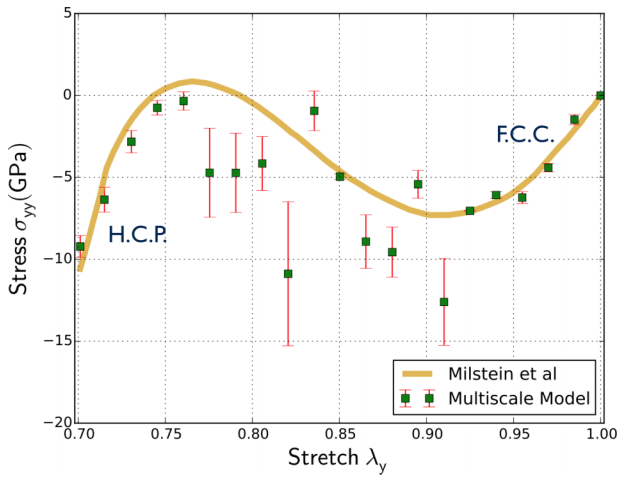

FIG. 10. Stress-strain relation under uniaxial displacement loading. The data are compared with the theoretical prediction by Milstein and Farber.[34]

the solid curve is the theoretical result, and the data collected from the internal cell during the simulation is marked by error bar. The data are obtained by averaging three calculations under similar situations to obtain more reliable results. Overall, the simulation agrees well with the theoretical result. However, in the range of [0.75 0.9], large deviation is observed between the curves. This is the transition area between two structures if we check the energy landscape in Ref. 34. The structure is unstable in this range and an equilibrium state is hard to reach. Therefore, the measure of stresses is unreliable. In ranges [0.9 1.0] and [0.7 0.75], the results have better agreements with theoretical result. This is because in the stretch range [0.9 1.0] the crystal is in F.C.C. structure, and the deformation is completely elastic; and in the stretch range [0.7 0.75] range the crystal lattice has formed a stable H.C.P. structure, and the local deformation is also elastic in this range.

We plotted the stresses at $\lambda_y = 0.73$ and $\lambda_y = 0.97$ for different sizes of supercells in Fig. 11. These two stretches are in elastic range of H.C.P. and F.C.C. separately. Thus, they should be reliable to study the stress states. The size of the supercell ranges from $2 \times 2 \times 2$ to $7 \times 7 \times 7$ in unit cells.

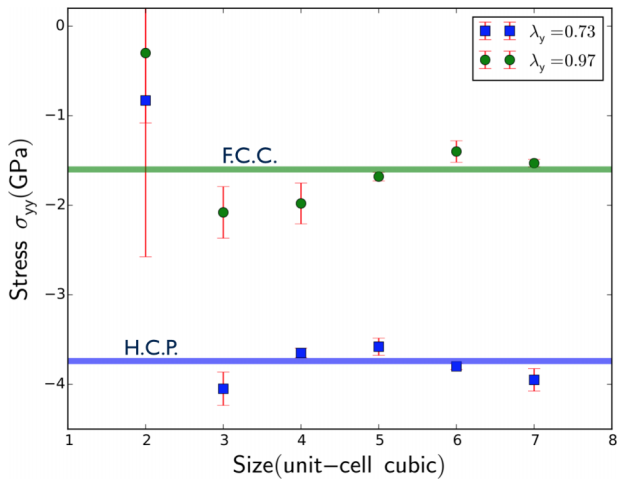

FIG. 11. Stress σ_{yy} for different sizes of supercells at stretches $\lambda_y = 0.73$ and $\lambda_y = 0.97$. Horizontal lines are theoretical results in Ref. 34 as benchmarks.

In Fig. 11, we observe no significant deviation when the supercell is larger than 3 unit-cell cubic. Sizes of supercells in this range should not influence the results. For problems such as elastic deformation and homogeneous phase transition in this example, we expect to have satisfactory results up to much larger size of supercells.

B. Test of traction boundary condition

In the second example, we studied the dynamic response and phase transition of the same nickel bulk under a constant surface traction boundary condition. The initial model is shown in Fig. 12(a). Same as before, the lattice structure is face centered cubic, and the finite-size bulk crystal contains $3 \times 3 \times 3$ supercells, and each supercell has $3 \times 3 \times 3$ unit cells. Total number of atoms is 2916. The weight of each nickel atom is 58.69 u. The lattice constant $a = 0.352$ nm, and the volume of the bulk is about 31.8 nm^3. The orientations of the faces are [100], [010], and [001], which correspond to x, y, and z coordinates, separately. During the entire procedure, the temperature was controlled around 350 K. We use the same Morse potential and integration algorithm as in the displacement example. The integration time steps used in this simulation are 0.0015 ps, 0.0012 ps, and 0.000 15 ps for different scales.

At the beginning of the calculation, the bulk is relaxed in a stress free state for 5000 steps to obtain the energy-minimizing configuration. The volume change of the bulk is less than 1% compared to the initial model. We then apply a compressive traction $\bar{\mathbf{t}} = 6$ GPa on the top and bottom surfaces of the bulk as shown in Fig. 12(a). The traction is a dead load throughout the simulation in [100] direction. Figs. 12(b)–12(d) show the snapshots of the loading history. At the beginning, i.e., $t < 2$ ps, the model is in a state of linear elastic deformation as observed in Fig. 12(b), where particles are stretched uniformly, and the structure stays nearly in F.C.C. Subsequently, phase transformation initiates at the top and bottom surfaces where the tractions are applied and propagate quickly to the center, as shown in Figs. 12(c) and 12(d). After about $t = 9$ ps, the entire bulk turns into the H.C.P. phase. Based on morphology of the final equilibrium configuration shown in Fig. 12(e), the original {001} planes in F.C.C. switch to {0001} closely packed planes in H.C.P. The phase transformation resulted in the new lattice constants $a = 0.25$ nm and $c = 0.41$ nm for the H.C.P. structure which is the same as in the example of displacement loading. And the structure is regular without boundary distortion.

We have observed the overall shape change of the final configuration. Although the new configurations are standard H.C.P. structures with both displacement and traction loading, a slight difference between the shapes of the bulk can be found. In the example of displacement boundary condition, the final H.C.P. bulk is a regular parallelepiped as in Fig. 9(c). When the traction boundary condition is applied, the bulk turns out to be a zigzag shape which can be observed in Fig. 12(e). This is a result of different orientations of interplanar slips. Theoretically, interplanar slip has no preference on directions. In practice, many factors can contribute to the difference, e.g., initial imperfection of the geometry, potential energy, and integration time steps.

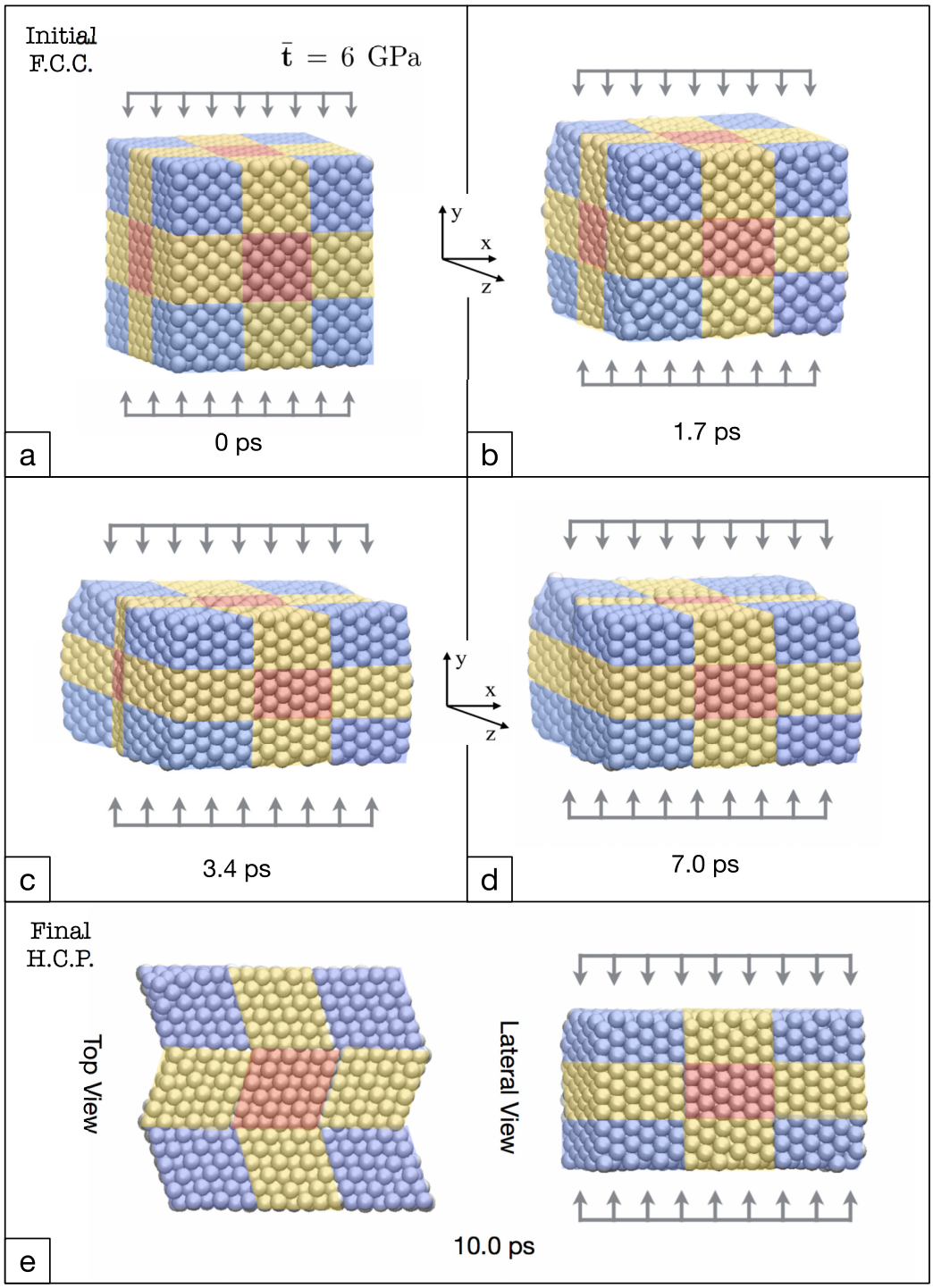

FIG. 12. Initial (a) and final (e) configurations of the model when a constant surface traction of $\bar{t} = 5$ GPa is symmetrically applied on its top and bottom surfaces, and snapshots (b)–(d) of the propagation of phase transition. Different colors are used to distinguish different cells.

We also analyzed the traction-stretch relation for the model and plotted the result in Fig. 13. As the compressive surface traction increases, the stretch decreases following the curve in path I. At some certain point around 5 GPa, the curve jumps to another path which is marked by red circles. These two paths are almost straight which reflect the linear elastic deformation of the two distinct structures of F.C.C. and H.C.P. as we discussed previously. As we unload the traction gradually from the new H.C.P. structure (path II), the curve goes straight up (path III) without jumping back to the original F.C.C. Apparently, the new H.C.P. bulk is stable under further loading/unloading. Different from displacement loading, the stress-strain curve with traction boundary has a break point because the model jumps over the unstable configurations. However, if displacement is controlled, the model still passes through unstable configurations between F.C.C. and H.C.P., but the measure of stress is unreliable. We can approximate the Young's modulus based on the curves in Fig. 13. E_1 is the Young's modulus for the initial F.C.C. structure on [010] direction, which is in the range of 150–220 GPa. E_2 and E_3

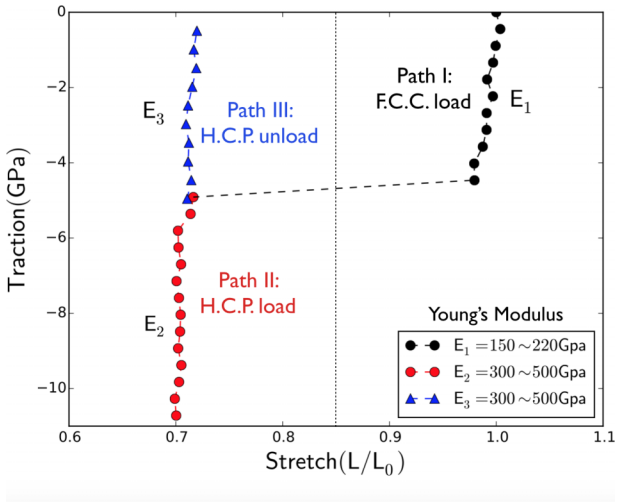

FIG. 13. Traction-stretch curve of the loading-unloading processes in equilibrium state.

are measured for the H.C.P. structure on $[11\bar{2}0]$ direction for loading and unloading procedures, respectively. They are in the range of 300–500 GPa.

VIII. SUMMARY AND DISCUSSIONS

In this paper, we have presented a systematic multiscale model based on the fundamental theory of molecular dynamics. The model includes the kinematics of multiscale structure, the force field, and the dynamics of different scales. For kinematics, we arranged and assembled information from atomistic level and smoothly transit to macroscopic level without any continuum assumption. Thus, the multiscale structure is completely equivalent to molecular dynamics. We partitioned the molecular domain to several subsystems and introduced the concept of supercell, which corresponds to the counterpart of "material point" in continuum mechanics. This little object has all kinds of motions found in "material point," i.e., rigid body translation, rotation, and stretch. Moreover, atomistic motion is reflected in the internal degrees of freedom. The structure extended the atomic model with chaotic particle motion to organized higher level motion. We then characterized the force field for the multiscale system, i.e., mechanical environment for each single supercell and the corresponding potential energy. We distinguished two kinds of forces due to their different origins, which are direct atomistic interaction in microscopic scale and macroscale mechanical loads such as surface traction and body force. This differentiation enriched the multiscale theory in the perspective of force characterization and provided possibility to introduce macroscale boundary conditions associated with kinematics. Based on the multiscale kinematics and force field, we derived dynamical motion for different scales. We discussed the driving force and resistant force for each scale based on the equations of motion and provided details for applying different macroscale boundary conditions.

The multiscale theory proposed is novel compared to other multiscale techniques and conventional molecular dynamics. Most multiscale techniques put emphasis on computing efficiency and try to piece together theories in different scales. The main pitfall of many multiscale theories and coarse grain models is their adaptation of empirical assumptions which bring unphysical issues to lower atomistic level even those assumptions are successful within their own scale. The objective of this work is to examine the multiscale simulation from physical perspective; thus, the model is derived based on first principle without any *ad hoc* assumption. The main purposes of this work are: (1) To reveal the universal multiscale structure of molecular dynamics, and (2) to apply macroscale boundary conditions to a molecular dynamics system. Therefore, in all three scales present, the proposed multiscale molecular dynamics will have the same number of degrees of freedom that conventional molecular dynamics has. Hence, it does not really save any computational cost. However, the multiscale structure discovered in this work may help us build novel multiscale computational algorithms that may save computing resource.

We presented two examples to demonstrate the multiscale theory on response of the models under different macroscale boundary conditions. For displacement loading, we used a bulk nickel with $3 \times 3 \times 3$ supercells where the internal cell was served for benchmark test comparing with theoretical results in infinite nickel lattice. The bulk metal went through phase transition from F.C.C. to H.C.P. structure as expected. The regular pattern on boundary showed the advantage of the multiscale method over classical molecular dynamics. The stress-strain curves agreed well with theoretical prediction in elastic ranges. And no significant difference was found among different sizes of cells which justified the size independency within some certain range. We also used the same model to calculate the dynamic evolution and phase transition with constant surface traction. The original F.C.C. structure turned into H.C.P. configuration when the compressive load exceeded a critical value which is similar to displacement loading. The stress-strain relation with loading-unloading process demonstrated the material property before and after the transformation, as well as the critical structure transition.

As fast development of computer technology, we may be empowered to handle macroscopic models with atomistic precision, and the need for such direct atomistic calculation will become essential and important. As an atomic-based continuum mechanics, the proposed multiscale model may find broad applications in nano-engineering, mechanical engineering, bioengineering, material science, and engineering. We expect the challenging cross-scale problems in all fields today to be solved in a proper manner with compatible multiscale theory. By understanding the fundamental multiscale physics, we can have chance to develop compatible multiscale techniques for the purpose of computational efficiency. Recall that the basic unit "supercell" can interact with both microscale and macroscale environments (boundary conditions). We may use it as a transit element between atomistic and macroscopic domains as in common multiscale techniques today. In macroscale domain, various models can be employed depending on different problems, e.g., finite element method, mesh free method, and dislocation dynamics. This is an ongoing research, and a preliminary work will be reported in a separate paper. Other extensions of the work, including exploring thermodynamical boundary conditions other than mechanical

loads, i.e., heat flows from macroscopic boundary and passes through molecular system, will be subsequently reported.

ACKNOWLEDGMENTS

Q. Tong is supported by a graduate fellowship from Chinese Scholar Council (CSC), and this support is greatly appreciated.

APPENDIX: DERIVATION OF MACROSCALE DYNAMIC EQUATION

In this appendix, we outline the derivation of macroscale dynamic equation with continuum deformation, which has been discussed in Ref. 35. We know that the continuum deformation gradient depends on the relative displacements of all centers of mass, which is

$$\mathbf{F}_\alpha = \mathbf{F}_\alpha(\{\mathbf{r}_\beta\}), \tag{A1}$$

where $\{\mathbf{r}_\beta\}$ represent a set of all centers of mass. Then we have

$$\dot{\mathbf{F}}_\alpha = \mathbf{F}_\alpha(\{\mathbf{r}_\beta\}, \{\dot{\mathbf{r}}_\beta\}). \tag{A2}$$

From Equation (A1), we also have

$$\dot{\mathbf{F}}_\alpha = \sum_\beta \frac{\partial \mathbf{F}_\alpha}{\partial \mathbf{r}_\beta}\dot{\mathbf{r}}_\beta. \tag{A3}$$

Therefore,

$$\frac{\partial \dot{\mathbf{F}}_\alpha}{\partial \dot{\mathbf{r}}_\alpha} = \frac{\partial \mathbf{F}_\alpha}{\partial \mathbf{r}_\alpha}. \tag{A4}$$

From Equation (A2), we can derive

$$\ddot{\mathbf{F}}_\alpha = \sum_\beta \left[\frac{\partial \dot{\mathbf{F}}_\alpha}{\partial \mathbf{r}_\beta}\dot{\mathbf{r}}_\beta + \frac{\partial \dot{\mathbf{F}}_\alpha}{\partial \dot{\mathbf{r}}_\beta}\ddot{\mathbf{r}}_\beta\right]. \tag{A5}$$

On the other hand, from Eq. (A3), the relation is

$$\ddot{\mathbf{F}}_\alpha = \sum_\beta \left[\frac{d}{dt}\left(\frac{\partial \mathbf{F}_\alpha}{\partial \mathbf{r}_\beta}\right)\dot{\mathbf{r}}_\beta + \frac{\partial \mathbf{F}_\alpha}{\partial \mathbf{r}_\beta}\ddot{\mathbf{r}}_\beta\right]. \tag{A6}$$

Comparing Eqs. (A5) and (A6) and using relation (A4), we get

$$\frac{\partial \dot{\mathbf{F}}_\alpha}{\partial \mathbf{r}_\alpha} = \frac{d}{dt}\left(\frac{\partial \mathbf{F}_\alpha}{\partial \mathbf{r}_\beta}\right). \tag{A7}$$

Recall the total deformation $\boldsymbol{\phi}_\alpha = \boldsymbol{\chi}_\alpha \cdot \mathbf{F}_\alpha$, then the time derivative is

$$\dot{\boldsymbol{\phi}}_\alpha = \dot{\boldsymbol{\chi}}_\alpha \cdot \mathbf{F}_\alpha + \boldsymbol{\chi}_\alpha \cdot \dot{\mathbf{F}}_\alpha. \tag{A8}$$

By knowing the fact that $\boldsymbol{\chi}_\alpha$ is an independent variable and using relations (A4) and (A7), we have

$$\frac{\partial \dot{\boldsymbol{\phi}}_\alpha}{\partial \dot{\mathbf{r}}_\alpha} = \boldsymbol{\chi}_\alpha \frac{\partial \dot{\mathbf{F}}_\alpha}{\partial \dot{\mathbf{r}}_\alpha} = \boldsymbol{\chi}_\alpha \frac{\partial \mathbf{F}_\alpha}{\partial \mathbf{r}_\alpha} = \frac{\partial \boldsymbol{\phi}_\alpha}{\partial \mathbf{r}_\alpha} \tag{A9}$$

and

$$\begin{aligned}\frac{\partial \dot{\boldsymbol{\phi}}_\alpha}{\partial \mathbf{r}_\alpha} &= \boldsymbol{\chi}_\alpha \frac{\partial \dot{\mathbf{F}}_\alpha}{\partial \mathbf{r}_\alpha} + \dot{\boldsymbol{\chi}}_\alpha \frac{\partial \mathbf{F}_\alpha}{\partial \mathbf{r}_\alpha} \\ &= \boldsymbol{\chi}_\alpha \frac{d}{dt}\left(\frac{\partial \mathbf{F}_\alpha}{\partial \mathbf{r}_\beta}\right) + \dot{\boldsymbol{\chi}}_\alpha \frac{\partial \mathbf{F}_\alpha}{\partial \mathbf{r}_\alpha} \\ &= \frac{d}{dt}\left(\frac{\partial \boldsymbol{\phi}_\alpha}{\partial \mathbf{r}_\alpha}\right) = \frac{d}{dt}\left(\frac{\partial \dot{\boldsymbol{\phi}}_\alpha}{\partial \dot{\mathbf{r}}_\alpha}\right).\end{aligned} \tag{A10}$$

We rewrite Lagrangian here as

$$\begin{aligned}\mathcal{L}_\alpha = &\frac{1}{2}M_\alpha \dot{\mathbf{r}}_\alpha \cdot \dot{\mathbf{r}}_\alpha + \frac{1}{2}\dot{\boldsymbol{\phi}}_\alpha^T \dot{\boldsymbol{\phi}}_\alpha : \mathbf{J}_\alpha + \frac{1}{2}\mathbf{C}_\alpha : \sum_i m_i \dot{\mathbf{s}}_i \otimes \dot{\mathbf{s}}_i \\ &- \frac{1}{2}\sum_{i,j\in\alpha}\varphi(r_{ij}) - \sum_{i\in\alpha, j\notin\alpha}\varphi(r_{ij}) \\ &+ S_\alpha^0 \bar{\mathbf{t}}_\alpha \cdot \mathbf{r}_\alpha + \Omega_\alpha^0 \bar{\mathbf{b}}_\alpha \cdot \mathbf{r}_\alpha.\end{aligned} \tag{A11}$$

We have

$$\begin{aligned}\frac{d}{dt}\left(\frac{\partial \mathcal{L}_\alpha}{\partial \dot{\mathbf{r}}_\alpha}\right) &= \frac{d}{dt}\left(\frac{\partial \mathcal{L}_\alpha}{\partial \dot{\mathbf{r}}_\alpha} + \frac{\partial \mathcal{L}_\alpha}{\partial \dot{\boldsymbol{\phi}}_\alpha}\cdot\frac{\partial \dot{\boldsymbol{\phi}}_\alpha}{\partial \dot{\mathbf{r}}_\alpha}\right) \\ &= M_\alpha \ddot{\mathbf{r}}_\alpha + \frac{d}{dt}\left(\frac{\partial \mathcal{L}_\alpha}{\partial \dot{\boldsymbol{\phi}}_\alpha}\right)\cdot\frac{\partial \dot{\boldsymbol{\phi}}_\alpha}{\partial \dot{\mathbf{r}}_\alpha} \\ &\quad + \frac{\partial \mathcal{L}_\alpha}{\partial \dot{\boldsymbol{\phi}}_\alpha}\cdot\frac{d}{dt}\left(\frac{\partial \dot{\boldsymbol{\phi}}_\alpha}{\partial \dot{\mathbf{r}}_\alpha}\right)\end{aligned} \tag{A12}$$

and

$$\begin{aligned}\frac{\partial \mathcal{L}_\alpha}{\partial \mathbf{r}_\alpha} &= \frac{\partial \mathcal{L}_\alpha}{\partial \mathbf{r}_\alpha} + \frac{\partial \mathcal{L}_\alpha}{\partial \boldsymbol{\phi}_\alpha}\cdot\frac{\partial \boldsymbol{\phi}_\alpha}{\partial \mathbf{r}_\alpha} + \frac{\partial \mathcal{L}_\alpha}{\partial \dot{\boldsymbol{\phi}}_\alpha}\cdot\frac{\partial \dot{\boldsymbol{\phi}}_\alpha}{\partial \mathbf{r}_\alpha} \\ &= \sum_{i\in\alpha, j\notin\alpha}\mathbf{f}_{ij} + S_\alpha^0\bar{\mathbf{t}}_\alpha + \Omega_\alpha^0\bar{\mathbf{b}}_\alpha \\ &\quad + \frac{\partial \mathcal{L}_\alpha}{\partial \boldsymbol{\phi}_\alpha}\cdot\frac{\partial \boldsymbol{\phi}_\alpha}{\partial \mathbf{r}_\alpha} + \frac{\partial \mathcal{L}_\alpha}{\partial \dot{\boldsymbol{\phi}}_\alpha}\cdot\frac{\partial \dot{\boldsymbol{\phi}}_\alpha}{\partial \mathbf{r}_\alpha}.\end{aligned} \tag{A13}$$

The equations of motion for $\mathbf{r}_\alpha$ and $\boldsymbol{\phi}_\alpha$ are derived as

$$\frac{d}{dt}\left(\frac{\partial \mathcal{L}_\alpha}{\partial \dot{\mathbf{r}}_\alpha}\right) = \frac{\partial \mathcal{L}_\alpha}{\partial \mathbf{r}_\alpha}, \tag{A14}$$

$$\frac{d}{dt}\left(\frac{\partial \mathcal{L}_\alpha}{\partial \dot{\boldsymbol{\phi}}_\alpha}\right) = \frac{\partial \mathcal{L}_\alpha}{\partial \boldsymbol{\phi}_\alpha}. \tag{A15}$$

Considering the relations in Eqs. (A9), (A10), and (A15), last two terms in Eqs. (A12) and (A13) are cancelled when they are substituted into (A14). Finally, we have

$$M_\alpha \ddot{\mathbf{r}}_\alpha = \sum_{i\in\alpha, j\notin\alpha}\mathbf{f}_{ij} + S_\alpha^0\bar{\mathbf{t}}_\alpha + \Omega_\alpha^0\bar{\mathbf{b}}_\alpha \tag{A16}$$

which is identical as Equation (27).

[1]M. Praprotnik, L. D. Site, and K. Kremer, Annu. Rev. Phys. Chem. **59**, 545 (2008).
[2]J. Southerna, J. Pitt-Francisb, J. Whiteleyb, D. Stokeleyc, H. Kobashid, R. Nobesa, Y. Kadookad, and D. Gavaghan, Prog. Biophys. Mol. Biol. **96**, 60 (2008).
[3]S. Yip, Nat. Mater. **2**, 3 (2003).
[4]R. Car and M. Parrinello, Phys. Rev. Lett. **55**, 2471 (1985).
[5]P. Hohenberg and W. Kohn, Phys. Rev. **136**, B864 (1964).
[6]W. Kohn and L. J. Sham, Phys. Rev. **140**, A1133 (1965).
[7]S. O. Nielsen, C. F. Lopez, G. Srinivas, and M. L. Klein, J. Phys.: Condens. Matter **16**, R481 (2004).
[8]R. E. Rudd and J. Q. Broughton, Phys. Rev. B **58**, R5893 (1998).
[9]E. B. Tadmor, M. Ortiz, and R. Phillips, Philos. Mag. A **73**, 1529 (1996).
[10]V. B. Shenoy, R. Miller, E. B. Tadmor, D. Rodney, R. Phillips, and M. Ortiz, J. Mech. Phys. Solids **47**, 611 (1999).

[11]L. E. Shilkrot, R. E. Miller, and W. A. Curtin, Phys. Rev. Lett. **89**, 025501 (2002).
[12]L. E. Shilkrot, R. E. Miller, and W. A. Curtin, J. Mech. Phys. Solids **52**, 755 (1999).
[13]G. J. Wagner and W. K. Liu, J. Comput. Phys. **190**, 249 (2003).
[14]H. S. Park, E. G. Karpov, W. K. Liu, and P. A. Klein, Philos. Mag. **85**, 79 (2005).
[15]Y. Chen and J. Lee, Philos. Mag. **85**, 4095 (2005).
[16]L. Xiong, G. Tucker, D. L. McDowell, and Y. Chen, J. Mech. Phys. Solids **59**, 160 (2011).
[17]A. C. To and S. Li, Phys. Rev. B **72**, 035414 (2005).
[18]S. Li, X. Liu, A. Agrawal, and A. C. To, Phys. Rev. B **74**, 045418 (2006).
[19]W. E, J. Lu and J. Yang, Phys. Rev. B **74**, 214115 (2006).
[20]D. J. Evans and G. P. Morriss, *Statistical Mechanics of Nonequilibrium Liquids* (Cambridge University Press, England, 2008).
[21]H. C. Andersen, J. Chem. Phys. **72**, 2384 (1980).
[22]M. Parrinello and A. Rahman, Phys. Rev. Lett. **14**, 1196 (1980).
[23]M. Parrinello and A. Rahman, J. Appl. Phys. **12**, 7182 (1981).
[24]R. J. Asaro and V. Lubarda, *Mechanics of Solids and Materials* (Cambridge University Press, Cambridge, England, 2006).
[25]R. J. E. Clausius, Philos. Mag., Ser. 4 **40**, 122 (1870).
[26]D. P. Bertsekas, *Nonlinear Programming* (Athena Scientific, Cambridge, MA, 1999).
[27]J. P. Ryckaert, G. Ciccotti, and H. J. C. Berendsen, J. Comput. Phys. **23**, 327 (1977).
[28]C. Farhat and M. Lesoinne, Comput. Methods Appl. Mech. Eng. **182**, 499 (2000).
[29]L. Verlet, Phys. Rev. **159**, 98 (1967).
[30]C. W. Gear, Commun. ACM **14**, 176 (1971).
[31]S. Nosé, J. Chem. Phys. **81**, 511 (1984).
[32]W. G. Hoover, Phys. Rev. A **31**, 1695 (1985).
[33]F. Milstein, J. Appl. Phys. **44**, 3825 (1973).
[34]F. Milstein and B. Farber, Phys. Rev. Lett. **44**, 277 (1980).
[35]S. Li and Q. Tong, J. Appl. Phys. **117**(15), 154303 (2015).